Master's Theses

Theses and Dissertations

2023

Characterization of the Full-Length BAG3 Protein and Stress Induced Formation of BAG3-Z

Ahmed Gamal Abdalla Zied

Follow this and additional works at: https://ecommons.luc.edu/luc_theses

Part of the Molecular Biology Commons

LOYOLA UNIVERSITY CHICAGO

CHARACTERIZATION OF THE FULL-LENGTH BAG3 PROTEIN AND STRESS-

INDUCED FORMATION OF BAG3-Z

A THESIS SUBMITTED TO

THE FACULTY OF THE GRADUATE SCHOOL

IN CANDIDACY FOR THE DEGREE OF

MASTER OF SCIENCE

PROGRAM IN CELL AND MOLECULAR PHYSIOLOGY

BY

AHMED ZIED

CHICAGO, ILLINOIS

AUGUST 2023

ACKNOWLEDGEMENTS

بِسْمِ اللَّهِ الرَّحْمٰنِ الرَّحِيمِ

IN THE NAME OF ALLAH, THE COMPASSIONATE, THE MERCIFUL.

اقْرَأْ وَرَبُّكَ الْأَكْرَمُ، الَّذِي عَلَّمَ بِالْقَلَمِ، عَلَّمَ الْإِنْسَانَ مَا لَمْ يَعْلَمْ.

Read: And Your Lord Is The Most Generous. He Who Taught By The Pen. Taught Man What

He Never Knew.

— The Holy Quran, Surah al-Alaq 3:5

TABLE OF CONTENTS

LIST OF FIGURES

LIST OF TABLES

ABSTRACT

Bcl2-associated athanogene-3 (BAG3) is a pro-autophagy co-chaperone that we have previously shown localizes to the cardiac sarcomere and is critical for proteostasis and maintenance of normal sarcomeric function. Indeed, BAG3 loss in heart failure (HF) results in accumulation of ubiquitinated sarcomeric proteins, and depressed maximum force generating capacity (Fmax). However, how BAG3 is regulated in the cell is not well understood, with uncertainty about its structure and proteoforms.

During our analysis of human heart tissue, BAG3 appears as a "doublet", with one band at 74 kDa (BAG3-Z) and a second at a higher 85 kDa (BAG3-FL). Previous studies hypothesized the full-length BAG3 protein is 74 kDa, and the 85 kDa proteoform was due to phosphorylation. Our results confirmed that BAG3-FL is the full-length protein with a molecular weight of 85 kDa. It also revealed that BAG3-Z is a cleavage product of BAG3-FL at the N- and C- termini, which has not been reported before. We have shown that BAG3-Z formation is stress induced and caspase dependent, likely by caspases 1, 8, and 9. The N-terminus cleavage includes ~1/3 of the WW domain, suggesting a possible loss-of-function especially regarding autophagosome formation and regulation of the lysosomal degradation pathway. Furthermore, BAG3-Z preferentially localized to the myofilament compared to the cytoplasm, where it could be competing and inhibiting the activities of BAG3-FL. Identification of the specific cleavage sites in BAG3-FL, BAG3-Z's interactome, and its effects on the cardiomyocyte protein quality control and stress response is necessary for the development of BAG3-based therapeutics for HF.

CHAPTER ONE

INTRODUCTION

Proteostasis: Maintaining Protein Health in the Cell and Its Implications in Cardiomyopathies.

Proteins are the workhorses of the cell, playing essential roles in all biological processes. However, the proper folding and function of these proteins is often challenged by various stressors such as changes in temperature, or nutrient availability, and environmental toxins [1-3]. Moreover, the production of misfolded or aggregated proteins can also result from genetic mutations or errors during transcription and translation [3]. To counteract these challenges, and maintain normal cellular function and homeostasis, cells have developed intricate protein quality control (PQC) mechanisms to maintain proteostasis [4]. The maintenance of proteostasis is critical for cellular homeostasis, and dysfunction of this process has been implicated in numerous diseases, including neurodegenerative disorders, cancer, and cardiomyopathies [2, 3, 5].

Proteostasis involves a network of pathways that govern protein synthesis, folding, trafficking, and degradation [1, 6]. At the core of this network are molecular chaperones and folding catalysts that assist in the folding and refolding of proteins. Nascent and misfolded proteins are bound by chaperons that hydrolyze ATP and provide an appropriate environment for the proteins to undergo unfolding/folding cycles until the native folding state is achieved [7]. Proteins that are damaged beyond refolding are degraded and replaced with new proteins. Damaged proteins are marked for degradation by the addition of ubiquitin to lysine residues in

their amino acid structure which is recognized by the degradation machinery [8-10]. There are two main degradation pathways that remove misfolded and terminally damaged proteins, the ubiquitin-proteasome system (UPS) and the autophagy-lysosome pathway (ALP) [6, 8, 11]. In UPS, the proteosome recognizes the ubiquitin signature on target proteins and degrades them into small peptides that are recycled back into amino acids and reincorporated into new proteins. This process utilizes ATP and only degrades single proteins that are unfolded [3]. The autophagsome-lysosomal pathway (ALP) is known for degrading whole organelles and protein aggregates. In ALP, a membrane known as the phagophore forms around damaged proteins and organelles. Once this membrane is fully developed into a vacuole containing the cargo to be degraded, it is referred to as the autophagosome [12, 13]. The autophagosome then fuses with the lysosome, an acidic vacuole containing various proteases and hydrolases that degrade the contents of the autophagosome [8]. The importance of proteostasis in cellular health and disease has garnered significant attention in recent years. A growing body of evidence suggests that disruptions in proteostasis can lead to the accumulation of misfolded or aggregated proteins, resulting in cellular toxicity and disease pathogenesis [13, 14].

The sarcomere, the basic contractile unite of cardiomyocytes, is under constant mechanical stress, making its proteins more prone to misfolding and aggregation [4, 15]. Since cardiomyocytes are non-renewing, refolding or degrading and replacing these misfolded proteins is critical for maintaining uninterrupted sarcomere contractile function and the survival of cardiomyocytes. Research on animal models of cardiomyopathies, as well as heart tissue samples from cardiomyopathy patients, has shown a strong correlation between the accumulation of ubiquitinated misfolded proteins and reduced heart functions [10, 15-19]. Proteasome inhibition in healthy pigs lead to hypertrophic-restrictive cardiomyopathy phenotypes. On the tissue level,

there was a significant accumulation of ubiquitinated proteins, apoptosis, and fibrosis [16]. Proteasome inhibitors used for cancer treatment, such as Velcade and Carfilzomib, has shown clinical cardiotoxic effects as well [20-23]. Levels of UPS enzymes and overall levels of ubiquitin were significantly increases in human DCM heart samples compared to healthy samples [18]. Several mechanisms have been proposed to tie the accumulation of ubiquitinated proteins and cardiomyopathy, including oxidative stress, ER stress, decreased removal of apoptotic proteins, protein aggregates, and altered cell signaling [14, 15, 18, 19]. Ubiquitinated proteins were also shown to remain embedded in the z-disks of the sarcomere, impairing the contractility of cardiomyocytes [24]. This accumulation of misfolded proteins and contractile dysfunction correlated with a reduction in the anti-apoptotic pro-autophagy protein, BAG3 (Bcl-2 Associated Athanogene 3) [24-26].

The Co-chaperone Bcl-2 Associated Athanogene-3

Bcl-2 Associated Athanogene-3 (BAG3) is a protein that belongs to the BAG family of proteins. These proteins are known for their interaction with heat shock protein 70 (HSP70), a molecular chaperone that plays a crucial role in protein folding and degradation, through their C-terminus BAG domain. BAG3 is unique because it has four different domains and protein interaction regions: the tryptophan-tryptophan domain (WW), two isoleucine-proline valine (IPV) motifs, a proline-rich (PxxP) region, and the BAG domain (Figure 1) [3, 13, 27, 28].

BAG3 is involved in many essential cellular processes, including apoptosis, autophagy, and development, through these domains and protein interactions [28-32]. Disruption of BAG3 functions, due to complete or partial loss of one or more of its domains, has detrimental effects on cell survival [33-36]. Various studies have shown significant reduction in BAG3 levels in the failing human heart and animal models of heart failure (HF) [24-26]. Similarly, a reduction in

cardiac function was observed in a heterozygous BAG3 knockout mouse model, correlating with

increased accumulation of ubiquitinated proteins. This phenotype was rescued by BAG3 gene

therapy using rAAV9-driven BAG3 expression, confirming the cardioprotective role of BAG3

and establishing possibilities for BAG3-based therapies for heart failure [24].
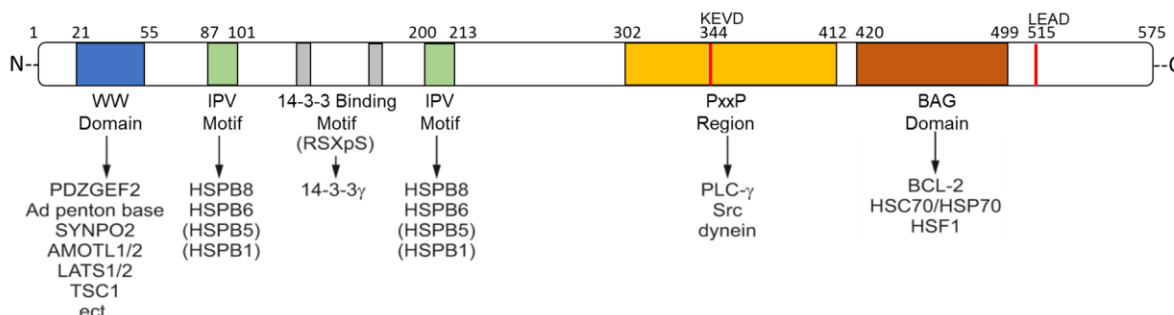
Figure 1. BAG3 Protein Structure and Domains. BAG3 is a co-chaperone protein that plays
an essential role in several cellular processes, including apoptosis regulation, autophagy,
cytoskeleton remodeling, and development. It comprises four domains and motifs that dictate its
activity and protein interactions. The WW domain interacts with proteins involved in autophagy
and lysosomal degradation of ubiquitinated proteins, the IPV motifs promote interactions with
small heat shock proteins, the proline-rich region (PXXP) facilitates interactions with
phospholipase C gamma, SRC, and dynein, and is critical for BAG3's cell protective effects.
Finally, the C-terminus BAG domain interacts with Bcl-2, to inhibit apoptosis, and
HSP70/HSC70, regulating HSP70 client processing and autophagy.

BAG3 Domains and Protein Interactions

The WW domain, comprising approximately 40 amino acids located at the N-terminus of

BAG3, is a crucial component of its protein-interacting regions. It features two conserved

tryptophan residues, spaced by 20-23 amino acids, which bind proline-rich motifs in target

proteins [27]. Through the WW domain, BAG3 interacts with a diverse set of proteins, involved

in protein turnover and autophagy [28, 37, 38]. BAG3's interaction with components of the

Hippo signaling pathway, such as LATS1 and AMOLT1, is essential for cell proliferation, the

stress response, and lysosomal protein degradation [32, 39, 40]. The WW domain also facilitates

BAG3's interaction with autophagosome membrane protein LC3 and SYNPO2, enabling BAG3 to recruit LC3 to the site of autophagosome formation [38, 41]. Additionally, the WW domain plays a crucial role in BAG3's interaction with the adaptor protein p62, which selectively delivers ubiquitinated proteins to the autophagosome for degradation. Overall, the WW domain is a key domain of BAG3 that mediates its ability to interact with diverse sets of proteins involved in the autophagosome-lysosome degradation pathway [30].

BAG3's N-terminal region downstream from the WW domain contains two conserved Isoleucine-Proline-Valine (IPV) motifs, which are essential for interacting with various small heat shock proteins such as HSPB8 (HSP22) and HSPB6 (HSP20) [30, 42]. BAG3 also interacts with HSPB5 (αB-crystallin) and HSPB1 (HSP27), although to a lesser extent [3]. Small heat shock proteins do not have folding abilities. Instead, they bind and stabilize proteins, prevent aggregation, and help other heat shock proteins bind their clients [24, 42, 43]. The interaction between BAG3 and HSPB8 is critical for regulating cellular processes such as proteostasis, stress response, and autophagy [3, 44, 45]. BAG3 acts as a co-chaperone to enhance HSPB8's activity and stability, which in turn promotes the refolding or degradation of misfolded and damaged proteins [46]. Additionally, BAG3 contains a 14-3-3 binding motif located between these two IPV motifs, allowing BAG3 to bind 14-3-3 γ, which acts as a molecular adaptor for the BAG3-dynein interactions [3, 29, 47].

The proline-rich domain (PxxP) of BAG3, located upstream of its C-terminus BAG domain, is critical for BAG3's interaction with HSC70 in order to maintain its levels and anti-apoptotic activities [34]. Furthermore, the PxxP domain mediates binding to proteins containing an SH3 domain, such as phospholipase C gamma (PLC-γ), allowing BAG3 to regulate the phosphorylation and activation of proteins involved in cell growth and proliferation [3, 48, 49].

Recently, the PxxP domain has also been shown to mediate the interaction between BAG3 and dynein. BAG3 promotes the binding of dynein to its cargo by interacting with the dynein intermediate chain (DIC), a component of the dynein motor complex [47, 50, 51]. This interaction may facilitate the recruitment of dynein to specific cargoes and modulate the directionality and velocity of cargo transport [52].

At its C-terminus, BAG3 contains the conserved 80 amino acid BAG domain. The BAG domain is essential for BAG3 to interact with the anti-apoptotic protein Bcl-2 and the ATPase domain of HSP70 [3, 27, 28, 30, 49, 53]. The interaction between BAG3 and Bcl-2 is important for regulating the stability of Bcl-2 and its ability to inhibit apoptosis. BAG3 regulates the protein folding activity of HSP70 and prevents the premature release of unfolded proteins from the Hsp70 chaperone complex, thereby ensuring efficient protein folding. BAG3 has also been shown to interact with the transcription factor Heat shock factor 1 (HSF-1), which allows BAG3 to regulate protein synthesis [54].

BAG3 and Selective Autophagy

Through an array of protein interactions, BAG3 is a key player in Chaperon Assisted Selective Autophagy (CASA), a selective process for degrading ubiquitinated proteins and damaged organelles [3, 5, 24, 50]. The CASA complex comprises HSP70, HSPB8, BAG3, CHIP, along with other proteins and cochaperones (Figure 2). BAG3 facilitates ubiquitination of the clients of HSP70 through its interaction with CHIP, which recruits autophagy proteins and adaptors such as LC3, SYNPO2, and p62 for the formation of the autophagosome and engulfment of the cargo [32, 40, 55, 56]. Moreover, BAG3 can chaperone and release its clients along microtubules through its interaction with dynein. This robust system ensures constant

turnover of misfolded proteins and damaged organelles and prevents toxicity from protein

aggregation.

CASA plays a critical role in the stress response of many cell types, such as skeletal

muscle and neurons, and its impairment causes different pathologies [3, 40, 41, 57-59]. For

example, BAG3 and CASA can degrade the pathological protein responsible for Huntington's

disease, Htt43Q, tying impairment of CASA to the fatal neurodegenerative disease [31]. In the

heart, the CASA complex localizes to the z-disk of cardiomyocytes' sarcomere, releasing

ubiquitinated misfolded proteins from the myofilament and sending them for degradation by the

autophagosome [24]. CASA is crucial for the turnover of critical sarcomeric proteins, such as

Filamin C and α-actinin, and the maintenance of proper sarcomere structure and function.
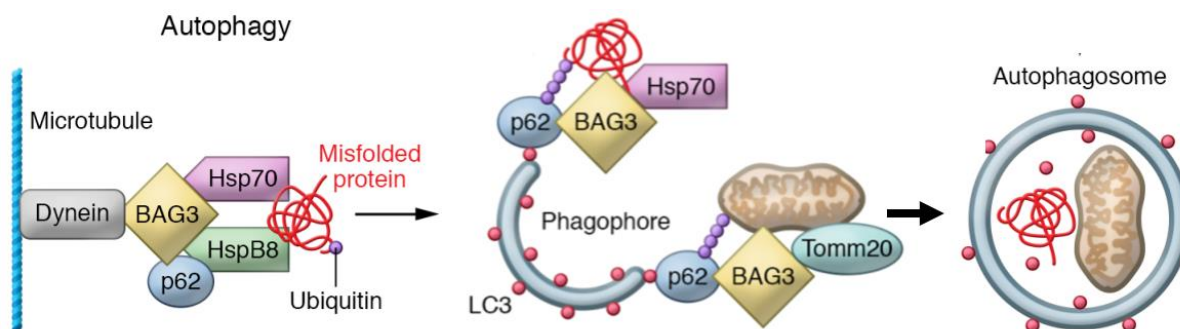
Figure 2. BAG3 is Involved in CASA to Regulate the Degradation of Damaged Proteins and Whole Organelles. BAG3 binds HSP70, HSPB8, HSPB6, CHIP, and other small heat shock proteins and co-chaperons to form the CASA complex that localizes to the z-disk of the sarcomere. The CASA complex binds misfolded proteins and transports them along microtubules, though BAG3's interaction with dynein, to the site of the autophagosome formation. BAG3 participates in the development of the phagosome into a mature autophagosome, though its SYNPO and LC3 interactions, and protein delivery into the autophagosome through its interaction with the protein p62. A fully mature autophagosome is formed carrying a cargo of misfolded proteins and damaged organelles for lysosomal degradation. Figure adapted from [39].

BAG3 Variants

BAG3's function is critically dependent on its domain and protein-interacting regions. As a result, BAG3 variants and mutants that lack essential functions may compromise the overall cellular protein quality control and stress response. To date, only one BAG3 splice variant has been identified. BAG3-202 (Ensemble, Uniprot) is a splice variant that occurs at multiple sites in the BAG3 transcript and codes for a 325 amino acid protein [60]. However, there is no information about how BAG3-202 was identified or the exact splicing sites. The protein product of BAG3-202 has not been observed in-vivo either.

Many disease related BAG3 mutations and variants have been identified and described in literature. These mutations are usually associated with different pathologies, such as muscle dystrophy, DCM, and sensorimotor neuropathy [57, 61-63]. All DCM-associated pathological mutations affect the WW domain, the second IPV motif, or the BAG domain, highlighting their important roles in BAG3's functions [49]. Qu et al. provide a comprehensive description and identification of the BAG3 mutations [49].

On the protein level, three BAG3 proteoforms have been reported in the literature. A 40 kDa C-terminus truncation of BAG3 has been observed in neural synaptosomes, but its function and mechanism of formation are still unknown (Figure 3A) [64]. Recent research revealed a caspase-dependent cleavage of BAG3 in response to proteasomal stress (Figire 3B) [33, 35, 36]. Caspase 3 cleaves BAG3 at 344KEVD to form a 40 kDa proteoform that is ineffective in mediating protein quality control and lost its antiapoptotic effects, further confirming the importance of BAG3 domains in dictating its activity [36]. It is unknown whether the stress-induced 40 kDa BAG3 proteoform and the proteoform observed in neurons are related. Additionally, an 85 kDa proteoform of BAG3 has been observed in various cell types and in

response to stressors such as heat shock and chemical toxicity [28, 65]. The shift in molecular weight is hypothesized to be a result of phosphorylation, given BAG3's several serine-rich motifs and 10 tyrosine residues [28, 66, 67].
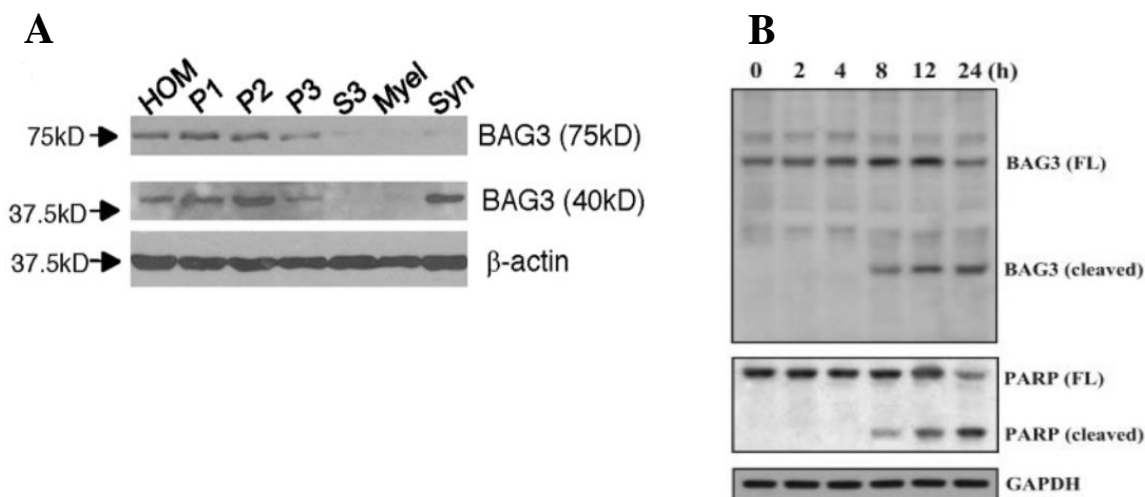
Figure 3. Previously Identified BAG3 Proteoforms. (A) Western blot for BAG3 in rat total brain homogenate (HOM), nuclear fraction (P1), fraction containing mitochondria, myelin and synaptosomes (P2), microsomal fraction (P3), Citosol (S3), Myelin (Myel), purified synaptosomal fraction (Syn). Figure adapted from [64]. **(B)** Western blot of BAG3 in SW1990 cells treated with10 mM of MG132 for the indicated times. Figure adapted from [36].

BAG3 Molecular Weight

BAG3's molecular weight has been a subject of uncertainty, with observations ranging from 74 kDa to 85 kDa, while the expected molecular weight is 62 kDa. By surveying 31 commercially available BAG3 antibodies (ThermoFisher Scientific, https://shorturl.at/juSW7), 20 reported BAG3 at a molecular weight between 80 and 90 kDa. For example, BAG3 antibodies from Bethyl Laboratories (A302-807A), Abnova (H00009531-M01A), Invitrogen (PA5-86741, PA5-18061, PA5-78292, PA5-120306, PA5-27696, PA5-54239, MA5-35563, MA5-33118, MA5-32706), Proteintech (10599-1-AP) all reported the molecular weight of BAG3 around 85 kDa. Eight different BAG3 antibodies from Abcam (ab47124, ab92309, ab209251, ab246224, ab246225, ab225561, ab193463, ab247535) report BAG3's molecular

weight at around 80 kDa. BAG3's molecular weight has also been inconsistent in literature. Some literature that studied BAG3 and analyzed it by western blotting doesn't report a molecular weight. Multiple papers report a molecular weight between 80 and 85 kDa, such as in Khalili et al. and Hohfeld et al. [38, 55, 65, 68]. Other literature reports a BAG3 "doublet" where two bands show on western blots with molecular weights between 74 kD and 85 kDa [24]. It has been assumed that the molecular weight of the full-length native BAG3 is 74 kDa and the 80-85 kDa proteoform was hypothesized to be a result of phosphorylation [28, 66, 67]. Although BAG3 can be phosphorylated at various sites, this theory is yet to be tested and confirmed. The ambiguity of BAG3's molecular weight highlights a significant topic that needs to be addressed regarding identifying the structure of the full-length BAG3, the mechanism of formation of its proteoforms, and the implications of the formation of those proteoforms on BAG3's function.

In our study, we analyzed BAG3 in different cell lines and tissue types and observed the BAG3 doublet in human atrial and ventricular tissue. The results of our work confirmed that the full-length form of BAG3 (BAG3-FL) has a molecular weight of 85 kDa, while the 74 kDa proteoform (BAG3-Z) results from cleavage at both the N and C termini of BAG3-FL, which has not been previously reported. Our analysis indicates that this truncation is stress-induced and caspase-dependent, which might compromise BAG3-Z's cardioprotective functions. It also poses a threat to BAG3-based therapies for HF as the introduced BAG3 would be susceptible to cleavage, reducing the effectiveness of such therapies. Therefore, understanding BAG3's structure, regulation, and proteoforms provides valuable insights for the end goal of developing therapeutic interventions for PQC dysfunction-related myopathies.

CHAPTER TWO

MATERIALS AND METHODS

Human Tissue Preparation

Human atrial and ventricular tissue samples, collected with Institutional Review Board

(IRB) approval with patient consent, were obtained from the Loyola University Chicago

Cardiovascular Research Institute Biorepository (CVRI). Non-failing (NF) tissue from donors

with no underlying cardiovascular disease were used to minimize interfering factors. Tissue was

cut and placed in 1mL Standard Rigor Buffer (SRB) with 30 µL of 10% Triton X-100 and 10 µL

of phosphatase and protease inhibitors to lyse and permeabilize the cells. Samples were

homogenized at 7000 RPMs 2-3 1 second pulses and then let sit on ice for 15 minutes. The lysate

was centrifuged at 200 g for 2 minutes to separate the cytoplasmic (supernatant) and the

myofilament (pallet) protein fractions. The myofilament fraction was resuspended in 1 mL of

SRB and clarified by centrifugation at 17,000 g for 2 minutes, resuspended in 9M urea (20

µL/mg), and sonicated. The cytoplasmic fraction was clarified by centrifugation and sonicated.

Myofilament fraction was centrifuged again at 17,000 g for 10 minutes at room temperature for

clarification and supernatant was transferred to a clean tube. Tissue lysates were aliquoted and

stored at -80°C. For the alkaline phosphatase treatment, tissue samples were prepped as

described without the addition of phosphatase inhibitor in the SRB buffer. Before the clarifying

centrifugation step, 10 µL of alkaline phosphatase (EF0651, Thermo Fisher Scientific) was

added to tissue lysates and incubated at 37°C for 2 hours. Following the phosphatase treatment, myofilament fraction was clarified by centrifugation, resuspended in 9M urea, and sonicated.

Chloroform Methanol Precipitation

Proteins from the cytoplasmic fraction were precipitated and resuspended in 9M urea to match the myofilament fraction. A volume containing 150 ug of protein was calculated and measured for each sample. 400 µL of Methanol, 100 µL Chloroform, and 300 µL of HPLC water were added and the samples were vortexed after the addition of each reagent. Samples were centrifuged at 14,000 g for 10 minutes yielding two aqueous layers with a solid protein layer in between. The top aqueous layer was removed, 400 µL of methanol was added and vortexed. Samples were centrifuged again at 14,000 g for 10 minutes. After removing the supernatant, samples were left to dry out at room temperature and then resuspended in an appropriate volume of 9M urea. Thermo BCA Protein Assay Kit was used to quantify the protein concentration of each sample.

BCA Protein Concentration Assay

The Pierce^{TM} BCA protein Assay Kit (23225, Thermo Fisher Scientific) was utilized to determine the protein concentrations. BSA standards were prepared and serially diluted based on the concentrations provided in the kit. For each samples analyzed, 2.5µL were pipetted into a 96-well plate, and 22.5µL of ddH2O was added to attain a final 10-fold dilution. Triplicates of each sample were prepared on the plate. The assay reagent was prepared by mixing Reagent A and Reagent B (provided in the kit) at a ratio of 50:1. Then, 200µL of the assay reagent was added to each well using a multichannel pipet. The plate was incubated at 37°C for 30 minutes. The CLARIOstar plate reader (BMG LabTech) was used to read the plate at 562nm. Standard curves

were created using BSA standards and the concentrations of the samples was calculated by

interpolation.

Western Blotting

Samples were prepared by mixing 10uL of sample with 8uL of SDS Tris-Glycine Buffer

(Life Technologies) and 2uL of Bolt Reducing Buffer (Fisher Scientific) then incubated at 99°C

for 10 minutes. A volume containing 10ug of protein from each sample was calculated and

loaded on a BoltTM 4-12% 28 Bis-Tris plus gel (NW04122BOX, Thermo Fisher Scientific). The

gel was run in running buffer at 150 volts for 45 minutes. The gel was transferred on a

nitrocellulose membrane (Thermo Scientific) by wet transfer at 10 volts for 1 hour. The

membrane was exposed to Revert Total Protein Stain (LI-COR Biosciences) for 5 minutes then

blocked in 2.5% Bovine Serum Albumin (BSA) in TBS for 1 hour with gentle rocking at room

temperature. The membrane was then incubated with the following primary antibody at the

indicated dilution in 2.5% Bovine Serum Albumin (BSA) in TBS with 0.1% Tween at 4°C

overnight: BAG3 (10599-1AP, Proteintech, 1:1,000), BAG3 N-terminus (MA5-35563, Thermo

Scientific), BAG3 C-terminus (PA5-53818, Invitrogen), p-TnI (4004S, Cell Signaling). A

complementary secondary antibody was added the next day and incubated at room temperature

for 1 hour: Anti-Rabbit IgG Polyclonal Antibody (926-32213, LI-COR Biosciences), Anti-

Mouse IgG Polyclonal Antibody (926-32212, LI-COR Biosciences). Azure Sapphire™

Biomolecular Imager was used to image the membrane and Image Studio Light (LI-COR

Biosciences) was used for analysis.

Immunoprecipitation (IP)

50 µL of Dynabeads Protein G (10003D, Thermo Fischer Scientific) were incubated with

5 µg of BAG3 antibody 10599-1AP, Proteintech) in 200 µl TBS with 0.1% Tween (TBS-T) for

20 min at room temperature with rotation. The immunocomplex was washed three times with

100 mM sodium borate (pH 9) and then the antibody was crosslinked to the beads by adding 1

mL of 20 mM dimethyl pimelimidate dihydrochloride (DMP) in 100 mM sodium borate for 30

min at room temperature with rotation. After crosslinking, the complex was blocked with 1 mL

of 200 mM ethanolamine (pH 8) for 2 hours to limit nonspecific protein binding. After blocking,

the immunocomplex was washed three times with 1 mL of IAP buffer (50 mM MOPS (pH 7.2),

10 mM sodium phosphate, 50 mM NaCl) and then resuspended in a volume containing 500 ug

myofilament-enriched protein lysates. After incubation for 10 min at room temperature with

rotation, the immunocomplex was washed six times with 1 mL of TBS-T on a magnetic rack.

Immunoprecipitated proteins were eluted by suspending the beads in 30 µL SDS buffer and 5 µL

reducing buffer and boiling at 100°C for 10 minutes. The eluant was directly loaded on a

BoltTM 4-12% 28 Bis-Tris plus gel (NW04122BOX, Thermo Fisher Scientific), run at 150 volts

for 45 minutes, and then Coomassie stained.

In-Gel Digestion and Protein Purification

The Coomassie stained gel was de-stained using a de-staining solution (50% Methanol,

40% water, 10% Acetic Acid) and BAG3 gel bands were cut. The gel cutouts were reduced by

incubating with enough volume of 250 mM DTT to cover them for 1 hour with shaking at 600

RPM, then alkylated using enough volume of 50 mM iodoacetamide (IAA) for 45 minutes. The

protein content from each gel cutout was digested using 2 ug of Trypsin/LysC protease overnight

at 37°C with shaking at 600 RPM. Peptides were extracted from the gel cutouts by incubating

with enough volume of 50% Acetonitrile (ACN) and 5% Formic Acid (FA) for 20 minutes at

25°C with shaking at 600 RPMs. Peptides were precipitated by vacuum centrifugation and

resuspended in 0.1% FA solution in HPLC water. Samples were cleaned up using C18 spin

columns (786-930, G Biosciences) and the peptide concentration of each sample was quantified using Pierce Quantitative Colorimetric Peptide Assay kit according to the manufacturer's protocol.

In-solution Digestion

Cell and tissue lysates were reduced by incubating with 5 mM DTT (20 µL/mL) for 45 minutes and alkylated using 10 mM iodoacetamide (20 µL/mL) for 30 minutes. The proteins were then digested with 5 ug Trypsin/LysC protease overnight at 37 °C with shaking at 600 RPM. Trypsin digestion was attenuated by acidifying the solution (pH =<3) using TFA at 0.1% final volume. C18 spin columns (786-930, G Biosciences) were used to clean the samples from any detergents using the provided protocol. Samples were dried by vacuum centrifugation, resuspended in 30 µL in buffer A (3% acetonitrile, 0.1% formic acid), and peptide concentration was measured using Pierce Quantitative Colorimetric Peptide Assay kit.

Mass Spectrometry (MS/MS) Method

Purified peptides,1.0 ug, were loaded onto a Vanquish Neo UHPLC system (Thermo Fisher) with a heated trap and elute workflow with a c18 PrepMap, 5mm, 5uM trap column(P/N 160454) in a forward-flush configuration connected to a 25cm Easyspray analytical column(P/N ES802A rev2) 2uM,100A,75um x 25 with 100% Buffer A (0.1% Formic acid in water) and the column oven operating at 35 °C. Peptides were eluted over a 150 min gradient, using 80% acetonitrile, and 0.1% formic acid (buffer B), going from 4 % to 18% over 15 min, to 40% over 115 min, then to 65% over 20 min, and then kept at 99% for 10 min, after which all peptides were eluted. Spectra were acquired with an Orbitrap Eclipse Tribrid mass spectrometer with FAIMS Pro interface (Thermo Fisher Scientific) running Tune 3.5 and Xcalibur 4.5. For all acquisition methods, spray voltage set to 2000V, and ion transfer tube temperature set at 300 oC,

FAIMS switched between CVs of −45 V, – 55 V, and −65 V with cycle times of 1.5s. MS1

spectra were acquired at 120,000 resolutions with a scan range from 375 to 1600 m/z,

normalized AGC target of 300%, and maximum injection time of 50ms, S-lens RF level set to

30, without source fragmentation and datatype positive and profile; Precursors were filtered

using monoisotopic peak determination set to peptide; included charge states, 2-7 (reject

unassigned); dynamic exclusion enabled, with n = 1 for 60s exclusion duration at 10 ppm for

high and low. DDMS2 scan using isolation mode   Quadrupole, Isolation Window (m/z):   1.6;

Activation Type set to HCD with 30%   Collision Energy (CE), Detector Type: Ion Trap; Scan

Rate: Turbo; AGC Target: 10000; Maximum Injection Time:35 ms, Microscans: 1 and Data

Type: Centroid.

MS/MS Data Analysis

For BAG3 sequence analysis, raw data were analyzed using FragPipe version 18.0,

MSFragger version 3.5, Philosopher version 4.4.0 (Alexey Nesvizhskii lab). The data were

searched against the human Uniprot protein sequence database (Home Sapiens Proteome ID

UP000005640). The search parameters included precursor mass tolerance of 20 ppm and 600

ppm for fragments, allowing two missed trypsin cleavages, oxidation (Met) and acetylation

(protein N-term) as variable modifications, and carbamidomethylation (Cys) as a static

modification.

For protein content and quantification, raw data were analyzed using Proteom

Discoveror 2.5 (Thermo Fisher) using Sequest HT search engines. The data were searched

against the Rattus norvegicus (Rat) UniProt protein sequence database (Proteome ID

UP000002494) or human (Home Sapiens Proteome ID UP000005640). The search parameters

included precursor mass tolerance of 10 ppm and 0.6 Da for fragments, allowing two missed

trypsin cleavages, oxidation (Met) and acetylation (protein N-term) and Phospho(+79.966, STY) as variable modifications, and carbamidomethylation (Cys) as a static modification. Percolator PSM validation was used with the following parameters: strict false discover rate (FDR) of 0.01, relaxed FDR of 0.05, maximum ΔCn of 0.05, and validation based on q-value. Precursor Ions Quantifier settings were Peptides to Use: Unique + Razor; Consider Protein Groups for Peptide Uniqueness set as True; Precursor Abundance Based On: Intensity; Normalization based on Total Peptide Amount; Scaling Mode set as none, low abundance peptides were removed by filtering out proteins with less than 3 PSMs, Protein Abundance Calculation based on the summed abundance of the connected peptide groups, and protein ratio was calculated as the median of all possible peptide ratios between replicates of all connected peptides, and T-test (background based) was used for class comparison. Differentially expressed proteins were selected based on p-value < 0.05 and log2 fold change > 1.0.

mRNA Isolation, cDNA synthesis, & PCR

Primers for each of the four exons of BAG3 were designed (Table 1) and obtained from Integrated DNA Technologies (IDT). Since it was hypothesized that BAG3-FL could be alternatively spliced at the beginning of exon 1 and the end of exon 4, exon 1 primers started at the 5' UTR and exon 4 primers extended into the 3' UTR. mRNA was isolated from human tissue samples using the RNeasy Fibrous Tissue Mini Kit (74704, Qiagen) and then cDNA was synthesized using the Thermo SuperScript™ IV Reverse Transcriptase kit (18-091-050, Thermo Fisher Scientific). PCR reactions were performed on the synthesized cDNA using primers for all 4 exons at a temperature gradient to ensure optimal results. The PCR products were run on a 1% or 2% agarose gel containing ethidium bromide (5 µL/100 mL) and imaged using Azure 300 imager.

Cell Culture

Neonatal Rat Ventricular Myocytes (NRVMs) were isolated from 0–1-day old neonatal

rat pups as described in [24]. NRVMs were plated on 10 mm cell culture plates coated with

gelatin and left for 1 day to attach to the surface. HeLa cells (84121901-1VL, Sigma-Aldrich)

were plated on 10 mm cell culture plates and left to attach for 1 day before splitting into multiple

plates.

Growth media for HeLa cells contained Fulbecco's Modified Eagle Medium (DMEM)

with 4.5 g/L glucose, 10% Fetal Bovine Serum, and 1% Pen-Strep. NRVM maintenance media

contained DMEM with 4.5 g/L glucose, 18.5% M199 medium, 10% Horse Serum (HS), 1%FBS,

1% Pen-strep, 1% ITSx, and 10 µM Brdu. Media was changed every 48 hours and cells were

kept at a confluency less than 80%. For cell collection, cells were lifted off the plates by

aspirating the media and incubating with 1.5 mL of Trypsin for 10 minutes. Cells were collected

and centrifuged at 1000 RPM for 5 minutes. The pallet was resuspended in 1 mL DBPS and

centrifuged again for clarification. Cells were then resuspended in 9M urea and sonicated. Cell

lysates were stored at -80°C.

Cell Stress Experiments

For proteasomal stress, HeLa cells were incubated with 10 mL of media containing 5uM

of MG132 at 37°C for 24 hours. Cells were then changed to normal media and left to recover

overnight. For heat shock, NRVMs were incubated at 42°C for 1.5 hours, and then left to recover

overnight at 37°C. For hypoxia and serum deprivation treatments, cells were incubated with low

serum DMEM media containing 1g/ml glucose and 1% FBS, for HeLa cells, and 1% HS with no

FBS for NRVMs. Cells were incubated in a hypoxic chamber (1% Oxygen, 5% CO_2, 94%

Nitrogen). Cells were then changed to normal media and left to recover overnight. For caspase

inhibition, cells were incubated with 40 µM of the pan-caspase inhibitor, Z-VAD(OH)-FMK, (ab120382, Abcam). For calpain inhibition, cells were incubated with 250 nM of the Calpain Inhibitor I (14921, Cayman Chemicals), or 20 µM of Calpeptin (ab120804, Abcam). Cells were incubated with the inhibitors for 2 hour prior to the stress treatment.

In-vitro BAG3 Cleavage

The caspase cleavage assays were conducted in a reaction buffer consisting of 50mM HEPES, pH 7.4, 100mM NaCl, 0.1% CHAPS, 1mM EDTA, 10% glycerol, 10mM DTT at a temperature of 37°C. 3 µg of human recombinant active caspase-1 (BML-SE168-5000, Enzo Life Sciences), caspase-3 (707-C3-010/CF, R&D Systems), caspase-7 (823-C7-010/CF, R&D Systems), and caspase-8 (705-C8-010/CF, R&D Systems) were used. Initially, the caspases were kept in the reaction buffer at 37°C for 5 minutes before the addition of 0.75 ug of recombinant human BAG3 (ab95384, Abcam), final total volume of 30 µl. After 3 hours, the reaction was halted by adding 30 µl of SDS-PAGE sample buffer and reducing agent mix, incubated at 99 °C for 10 minutes and 30 µl of the final mix was loaded on a gel and analyzed by western blotting.

Statistics

All data were analyzed using Microsoft Excel and GraphPad Prism 9.0 (Prism, CA). Western blots were analyzed using Image Studio™ Lite (LI-COR Biosciences). Experiments were conducted using at least three independent biological replicates, and the mean ± SEM of the results was reported. For datasets with three or more groups, one-way analysis of variance (ANOVA) was used as appropriate. For comparisons between two groups, the 2-tailed Student's t-test was employed. A p-value < 0.05 was regarded as statistically significant. ns $P > 0.05$, * $P \leq 0.05$, ** $P \leq 0.01$, *** $P \leq 0.001$, **** $P \leq 0.0001$.

Table 1. BAG3 Primers. Primers used for PCR reactions to test the hypothesis that BAG3-Z is a result of alternative splicing of the BAG3-FL mRNA. Primers were designed to cover each exon completely to be able to detect any splicing events in any of the four exons of BAG3-FL.

Primer	Sequence (5'-3')	Length	Location	Temperature	GC%
Mid of 5' UTR	CCGCCTTTAA TTCATAAAGG TGCC	24-mer	200 to 223	58°C	46% GC
Exon 1-R	TCGTTCCACG TAGTGGTGC	19-mer	498 to 480	59°C	58% GC
Exon 2-F	GCACCACTAC GTGGAACGA	19-mer	480 to 498	55°C	58% GC
Exon 2-R	TCAGAGGCA GCTGGAGAC T	19-mer	20,951 to 20,933	59°C	58% GC
Exon 3-F	AGTCTCCAGC TGCCTCTGA	19-mer	20,933 to 20,951	57°C	58% GC
Exon 3-R	GAAACAGGT GCAGTTTCTC GATG	23-mer	25,169 to 25,147	58°C	48% GC
Exon 4-F	CATCGAGAA ACTGCACCTG TTTC	23-mer	25,147 to 25,169	58°C	48% GC
Beg of 3' UTR	CCAAGTTACT GCATACCAA GCAG	23-mer	26,075 to 26,053	58°C	48% GC

CHAPTER THREE

RESULTS

The 85 kDa BAG3 Proteoform is not a Result of Phosphorylation.

The current literature has hypothesized that the normal full-length BAG3 protein is 74 kDa, while the 85 kDa proteoform is a product of BAG3 phosphorylation but this hypothesis has never been tested before [28, 66, 67]. BAG3 has many identified phosphorylation sites that regulate its functions and have implications in disease [3, 69]. However, it would take around 127 phosphorylation sites to account for the 10 kDa difference between the molecular weights of the two BAG3 proteoforms. Also the two BAG3 proteoforms appear as two clean and distinct bands, which is not typical for how phosphorylated proteins appear on western blots. To test the phosphorylation hypothesis, we treated the human atrial and ventricular tissue samples, where we observed the BAG3 doublet, with an alkaline phosphatase. Human heart samples were homogenized in SRB/Triton-X homogenization buffer without the phosphatase inhibitor. The cytosolic and myofilament fractions were separated by centrifugation, the myofilament fraction was resuspended in the alkaline phosphatase buffer provided, and then divided into control and treatment groups. Treatment groups were incubated with 10 Units of the alkaline phosphatase at 37°C for 2 hours and control samples were incubated with water. Samples were centrifuged, resuspended in 9M urea, and analyzed by western blotting using BAG3 and serine 23/24 phosphorylated Troponin I (p-TnI) antibodies (Figure 4A). Levels of p-TnI were used as a positive control to confirm the activity of the alkaline phosphates. BAG3 and p-TnI were quantified and normalized to the total protein. The results showed a significant decrease in the

levels of p-TnI in the phosphatase-treated group compared to the controls, confirming the

activity of the alkaline phosphatase (Figure 4B). However, the phosphatase treatment failed to

resolve the BAG3 doublet and there was no significant difference in the levels of either BAG3

proteoforms between the control and treatment groups (Figure 4C&D). These results suggest that

the 85 kDa BAG3 is not a result of phosphorylation of the 74 kDa BAG3.
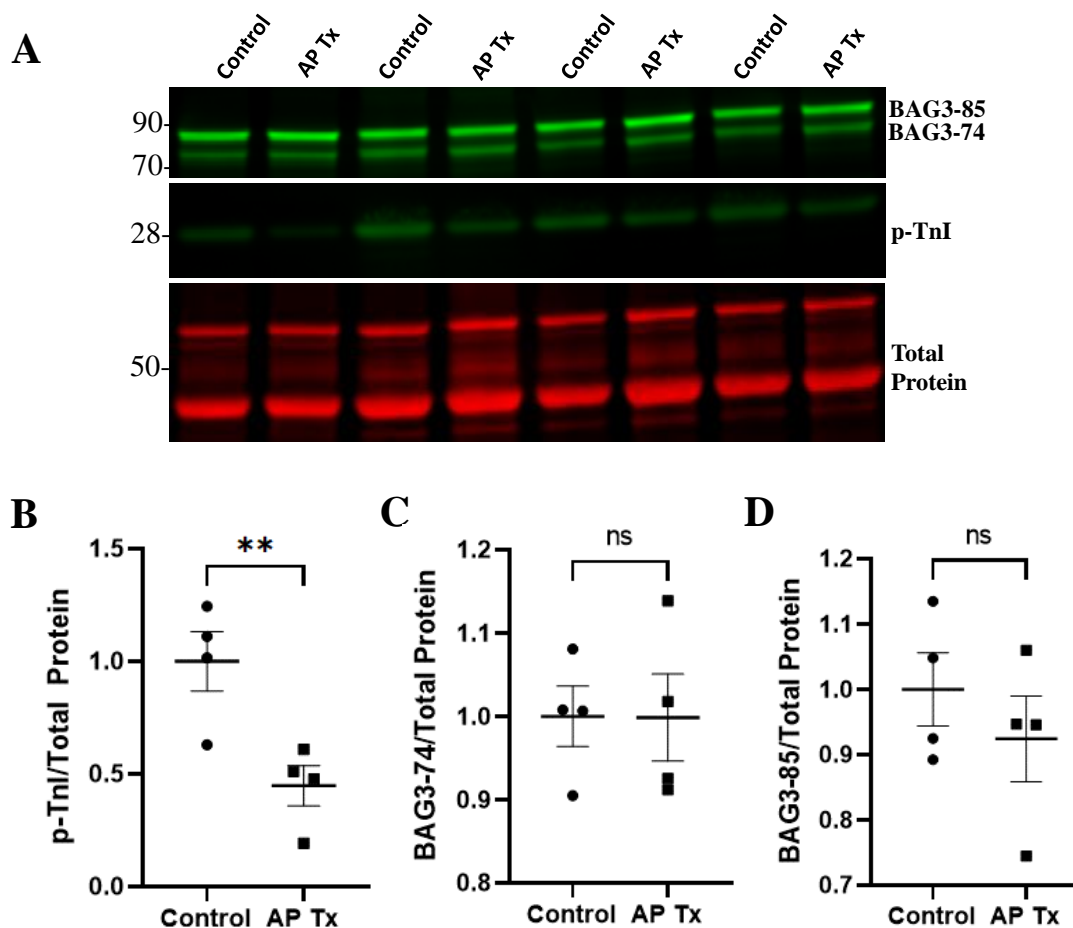
Figure 4. Treatment of Human Heart Tissue with an Alkaline Phosphatase Failed to Reduce the Intensity of the 85 kDa BAG3. (A) Western blot for BAG3 and p-TnI in the myofilament of control and alkaline phosphatase treated (AP Tx) human atrial and ventricular tissue samples. **(B)** Quantification of Ser23/24 p-TnI normalized to the total protein in control vs treatment samples; n = 4. **(C)** Quantification of the 74 kDa BAG3 (BAG3-74) normalized to the total protein in control vs treatment samples; n = 4. **(D)** Quantification of the 85 kDa BAG3 (BAG3-85) normalized to the total protein in control vs treatment samples; n = 4. Data are presented as mean ± SEM; two-tailed paired t-test.

BAG3-FL at 85 kDa is the Full Length BAG3.

Since the phosphatase treatment failed to reduce the 85 kDa BAG3, we hypothesized that the 85 kDa BAG3 proteoform (referred to as BAG3-FL hereafter) is the endogenous full-length form of BAG3 and the 74 kDa BAG3 proteoform (referred to as BAG3-Z hereafter) is a stable product of BAG3-FL truncation. To test this hypothesis, we started by surveying tissue samples from multiple species and analyzing BAG3's molecular weight, and we found BAG3 constantly appearing at around 85 kDa. In addition to the human samples where we initially observed the BAG3 doublet, 10 atrial and ventricular samples from 5 independent human donors were prepared for analysis. BAG3 was analyzed by western blotting in the whole tissue lysates and the two BAG3 proteoforms were observed in all the samples (Figure 5A). We analyzed BAG3 by western blotting in mouse and rat heart tissue, HeLa cells, and NRVMs (Figure 5B) as well as commercially purchased purified recombinant human BAG3 (rh-BAG3) (Figure 5C). In all the samples analyzed, we observed BAG3 at around 85 kDa. To add, the rh-BAG3 matched the 85 kDa BAG3 proteoform observed in the human tissue. Our observations suggested that BAG-FL is the full-length BAG3 protein and BAG3-Z is truncated product, either by alternative splicing or proteolytic cleavage.
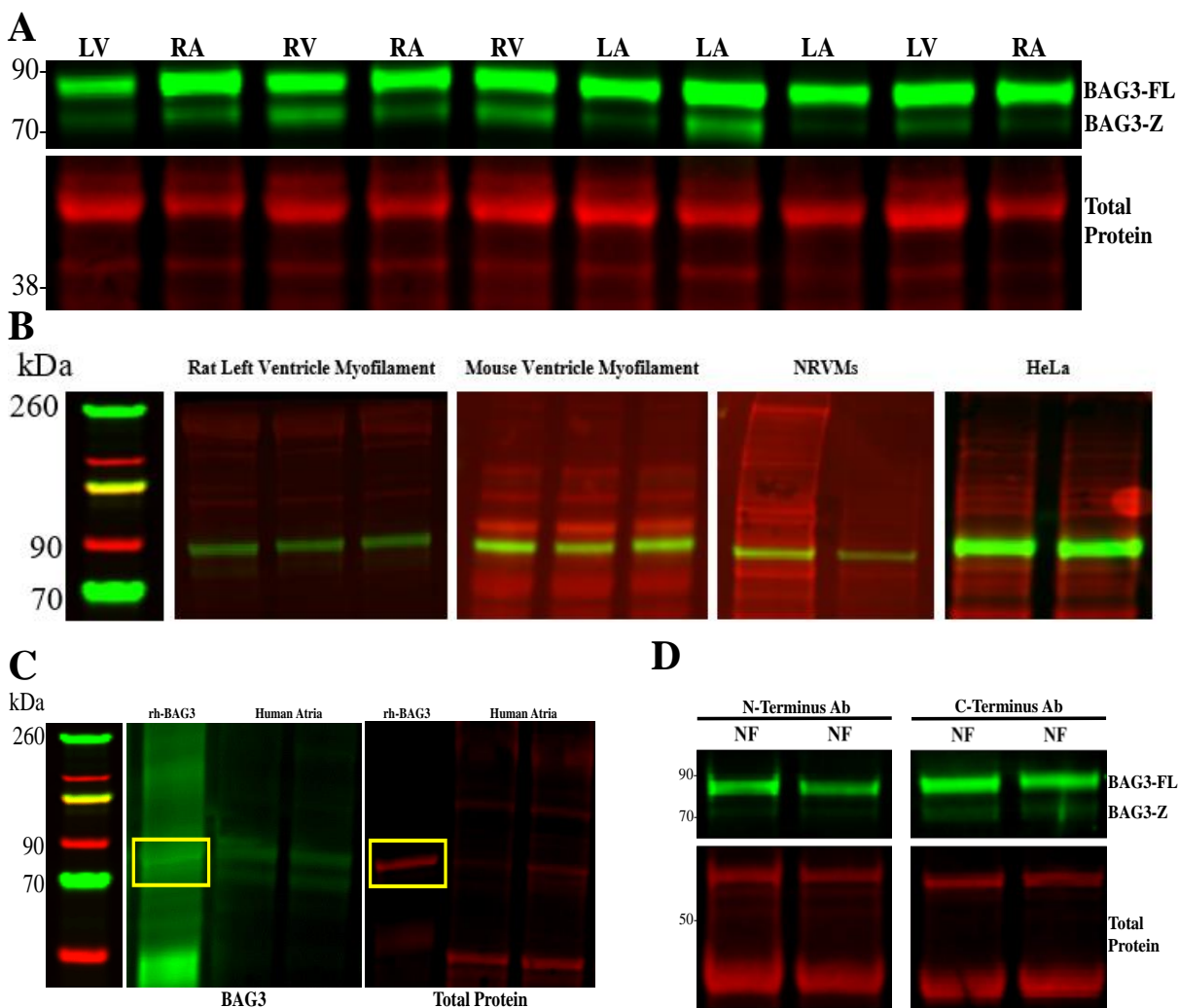
Figure 5. BAG3 from Mouse Heart Tissue, Rat Heart Tissue, NRVMs, HeLa cells, as well as Recombinant Human BAG3 All Match the Molecular Weight of BAG3-FL. (A) Western blot for BAG3 in human atrial and ventricular tissue from 5 independent donors; LV = left ventricle, LA = left atria, RV = right ventricle, RA = right atria. **(B)** Western blots for BAG3 in the myofilament of rat left ventricular tissue, the myofilament of mouse ventricular tissue, NRVMs, and HeLa cells; images are representative of 6 rat tissue samples, 8 mouse tissue samples, 5 NRVM samples, and 3 HeLa samples. **(C)** Western blot of purified recombinant human BAG3 (rh-BAG3, yellow box) from Abcam and BAG3 from human tissue samples; BAG3 antibody channel shown in green (left) and total protein stain channel shown in red (right); images are representative of 3 rh-BAG3 samples and 4 human tissue samples. **B & C:** images are aligned with the ladder used based on molecular weight. **(D)** Western blot for BAG3 in non-failing (NF) human heart tissue using N- and C- termini BAG3 antibodies; images are representative of 4 human heart samples.

BAG3-Z is not a Result of Alternative Splicing.

Alternative splicing is a molecular process by which different combinations of exons within a pre-mRNA transcript are selectively spliced together to produce multiple mRNA isoforms, each with a unique protein-coding sequence. This process enables a single gene to encode multiple proteins with distinct functions or properties, thereby increasing the diversity of the proteome without requiring an increase in the number of genes [70]. There is only one BAG3 splice variant that has been reported, referred to as BAG3-202, and it produces a 325 amino acids protein variant [60]. However, the function and physiological relevance of BAG3-202 has not been identified. Since we have shown that BAG3-Z is truncated at both the N- and C- termini, next we wanted to resolve the mechanism of this truncation. We first tested the hypothesis that BAG3-Z is formed by alternative splicing of the BAG3-FL transcript. To test this hypothesis, we utilized PCR experiments using custom made BAG3 primers (Table 1). The lost regions at the N- and C-termini of BAG3-Z correspond to parts of exon 1 and 4 of mRNA transcript of BAG3-FL, respectively. If BAG3-Z is a result of alternative splicing, there should be at least two mRNA products, with two different lengths, available for translation. We extracted BAG3 mRNA from human atrial and ventricular tissue, where we observed BAG3-FL and BAG3-Z, and used it to synthesize cDNA. We then designed primers for each of the four exons of BAG3-FL. The potential splicing sites would be at the beginning exon 1 and towards the end of exon 4. The primers for exon 1 were designed to start at the 5'UTR, covering the whole sequence of exon 1. Similarly, the primers for exon 4 extended into the 3'UTR, covering the full sequence of exon 4 (Figure 6A). By doing so and if BAG3-FL is spliced at exons 1 and 4, the products of the PCR reaction using the exons 1 and 4 primers should yield at least two products, corresponding to the spliced and non-spliced transcripts. Since both exons 2 and 3 are conserved in BAG3-FL

and BAG3-Z, we used them as controls to confirm the viability of our primers and the success of the PCR reactions. We preformed the PCR reactions, ran the products on an agarose gel containing ethidium bromide, and imaged on the Azure 200®. The products of the PCR reactions using the primers for exons 2 and 3 yielded one product for all samples tested, confirming that our PCR experiments were successful and that those two exons are conserved in BAG3-FL and BAG3-Z (Figure 6C&D). The products of the PCR reactions using the primers for exons 1 and 4 also yielded one product (Figure 6B&E). These results show that there is one BAG3 mRNA transcript available for translation which confirms that BAG3-Z is not a result of alternative splicing.
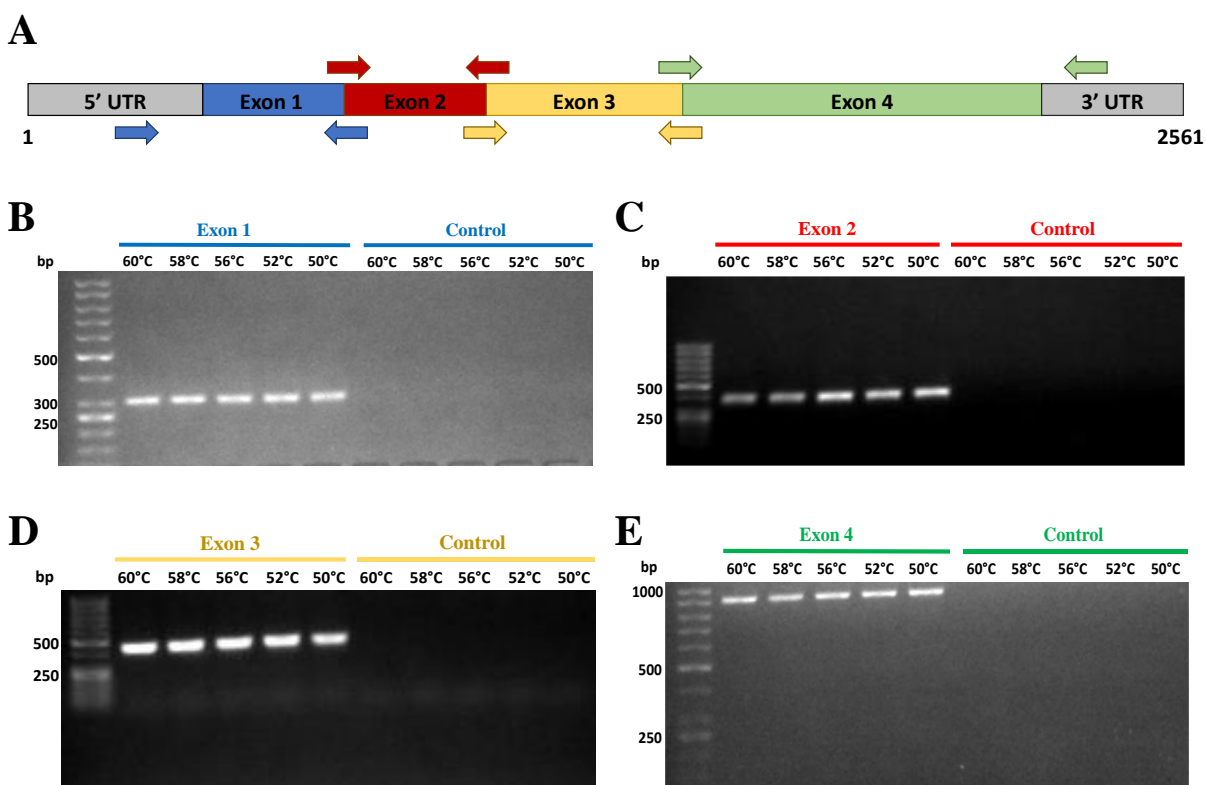
Figure 6. BAG3-Z Is Not a Result of Alternative Splicing of the BAG3-FL Transcript. (A) Schematic representation of the BAG3-FL mRNA (2561 bp) containing exons 1-4 as well as the 5'UTR and the 3'UTR; arrows represent the forward (pointing right) and reverse (pointing left) primers for each exon; blue = exon 1, red = exon 2, yellow = exon 3, green = exon 4. **(B)** PCR products using control (water) and exon 1 primers with cDNA synthesized using mRNA extracted from human atrial and ventricular tissue; expected weight of the PCR product = 257 bp; n = 5. **(C)** PCR products using control (water) and exon 2 primers with cDNA synthesized using mRNA extracted from human atrial and ventricular tissue; expected weight of the PCR product = 327 bp; n = 5. **(D)** PCR products using control (water) and exon 3 primers with cDNA synthesized using mRNA extracted from human atrial and ventricular tissue; expected weight of the PCR product = 402; n = 5. **(E)** PCR products using control (water) and exon 4 primers with cDNA synthesized using mRNA extracted from human atrial and ventricular tissue; expected weight of the PCR product = 883 bp; n = 5.

BAG-Z is a Stable Cleavage Product of BAG3-FL.

Since alternative splicing failed to explain BAG3-Z formation, we hypothesized that BAG3-Z is a stable prost-translational cleavage product of BAG3-FL. To test this hypothesis, we performed mass spectrometry analysis on BAG3-FL and BAG3-Z, as well as purified rh-BAG3, to determine their amino acid structures. BAG3-FL and BAG3-Z were immunoprecipitated from four atrial and ventricular tissue samples. The products of the immunoprecipitation, along with 0.5 µg and 0.75 µg of the rh-BAG3, were run on a polyacrylamide gel and the gel was stained with Coomassie protein stain to visualize the protein bands. The BAG3-FL and BAG3-Z gel bands were cut out and the proteins were extracted from the gel bands and prepared using an in-gel digestion protocol, cleaned up from any detergents using C18 spin columns, and analyzed by mass spectrometry. Excitingly, rh-BAG3 and BAG3-FL covered 93.7% and 90%, respectively, of the 575 amino acids of BAG3. BAG3-FL showed more than 97% homology to the amino acid structure of the rh-BAG3. These findings align with the western blot results that rh-BAG3 and BAG3-FL have the same amino acid structure and molecular weight (Figure 7A&B). Both the N and C-termini were conserved in the rh-BAG3 and BAG3-FL, with some missing sequences in-between, likely due to peptide loss during the sample preparation and the detection efficiency of

the mass spectrometer. On the other hand, BAG3-Z only covered 87.7% of the full BAG3 sequence (Figure 7C). By comparing the amino acids that were not covered in BAG3-Z to those in BAG3-FL and rh-BAG3, BAG3-Z appeared to be specially missing 29 amino acids from the N-terminus and 41 amino acids from the C-terminus in all the samples analyzed. Those sequences were present in all four BAG3-FL samples from two independent human myocardium and the two rh-BAG3 samples. Consistent with our hypothesis, our mass spectrometry results confirmed that BAG3-FL is the full-length BAG3, and BAG3-Z is a truncated proteoform, likely a product of post-translational cleavage. As part of the preparation protocol for mass spectrometry analysis, protein samples are digested by trypsin into small peptides to be loaded on the instrument, making it difficult to identify the exact cleavage site from the mass spectrometry results alone. However, the results indicate that BAG3-Z is cleaved at both the N-terminus, around the residue Isoleucine 30 (Ile30), and at the C-terminus, around the residue Lysine 533 (Lys533). These findings were further supported by western blot results of BAG3 in the same human atrial and ventricular tissue using antibodies specific for the N- and C- termini of BAG3. The epitope of the N-terminus antibody is between amino acids 50 and 150, and the epitope of the C-terminus antibody is between amino acids 466 and 575. Both antibodies recognized BAG3-Z to a much lesser extent compared to BAG3-FL, which supports results that BAG3-Z is cleavage at both the N- and C- termini (Figure 5D).

Our results confirm that the BAG3-FL is the endogenous full-length BAG3 with an observed molecular weight around 85 kDa. It also confirms that BAG3-Z is a product of BAG3-FL truncation at the N- and C termini, which has not been reported before. Although the C-terminus truncation does not reach the critical BAG domain of BAG3, it could possibly affect its function by altering its folding and interaction (Figure 7D). More importantly, almost 1/3 of the

WW domain is lost in BAG3-Z, raising the possibility of reduced function and protein interaction of BAG3-Z compared to BAG3-FL (Figure 7D). Since BAG3-Z is a stable product, it could also be competing with and hindering the activity of BAG3-FL, which would further paralyze the cardiomyocyte's PQC system and its stress response.

A

```
MSAATHSPMMQVASGNGDRDPLPPGWEIKIDPQTGWPFFVDHNSRTTTWNDPRVPSEGPKETPSSANGPSREGSRLP
PAREGHPVYPQLRPGYIPIPVLHEGAENRQVHPFHVYPQPGMQRFRTEAAAAAPQRSQSPLRGMPETTQPDKQCGQV
AAAAAAQPPASHGPERSQSPAASDCSSSSSSASLPSSGRSSLGSHQLPRGYISIPVIHEQNVTRPAAQPSFHQAQKT
HYPAQQGEYQTHQPVYHKIQGDDWEPRPLRAASPFRSSVQGASSREGSPARSSTPLHSPSPIRVHTVVDRPQQPMTH
RETAPVSQPENKPESKPGPVGPELPPGHIPIQVIRKEVDSKPVSQKPPPPSEKVEVKVPPAPVPCPPPSPGPSAVPS
SPKSVATEERAAPSTAPAEATPPKPGEAEAPPKHPGVLKVEAILEKVQGLEQAVDNFEGKKTDKKYLMIEEYLTKEL
LALDSVDPEGRADVRQARRDGVRKVQTILEKLEQKAIDVPGQVQVYELQPSNLEADQPLQAIMEMGAVAADKGKKNA
GNAEDPHTETQQPEATAAATSNPSSMTDTPGNPAAP
```
rh - BAG3

B

```
MSAATHSPMMQVASGNGDRDPLPPGWEIKIDPQTGWPFFVDHNSRTTTWNDPRVPSEGPKETPSSANGPSREGSRLP
PAREGHPVYPQLRPGYIPIPVLHEGAENRQVHPFHVYPQPGMQRFRTEAAAAAPQRSQSPLRGMPETTQPDKQCGQV
AAAAAAQPPASHGPERSQSPAASDCSSSSSSASLPSSGRSSLGSHQLPRGYISIPVIHEQNVTRPAAQPSFHQAQKT
HYPAQQGEYQTHQPVYHKIQGDDWEPRPLRAASPFRSSVQGASSREGSPARSSTPLHSPSPIRVHTVVDRPQQPMTH
RETAPVSQPENKPESKPGPVGPELPPGHIPIQVIRKEVDSKPVSQKPPPPSEKVEVKVPPAPVPCPPPSPGPSAVPS
SPKSVATEERAAPSTAPAEATPPKPGEAEAPPKHPGVLKVEAILEKVQGLEQAVDNFEGKKTDKKYLMIEEYLTKEL
LALDSVDPEGRADVRQARRDGVRKVQTILEKLEQKAIDVPGQVQVYELQPSNLEADQPLQAIMEMGAVAADKGKKNA
GNAEDPHTETQQPEATAAATSNPSSMTDTPGNPAAP
```
BAG3-FL

C

```
MSAATHSPMMQVASGNGDRDPLPPGWEIKIDPQTGWPFFVDHNSRTTTWNDPRVPSEGPKETPSSANGPSREGSRLP
PAREGHPVYPQLRPGYIPIPVLHEGAENRQVHPFHVYPQPGMQRFRTEAAAAAPQRSQSPLRGMPETTQPDKQCGQV
AAAAAAQPPASHGPERSQSPAASDCSSSSSSASLPSSGRSSLGSHQLPRGYISIPVIHEQNVTRPAAQPSFHQAQKT
HYPAQQGEYQTHQPVYHKIQGDDWEPRPLRAASPFRSSVQGASSREGSPARSSTPLHSPSPIRVHTVVDRPQQPMTH
RETAPVSQPENKPESKPGPVGPELPPGHIPIQVIRKEVDSKPVSQKPPPPSEKVEVKVPPAPVPCPPPSPGPSAVPS
SPKSVATEERAAPSTAPAEATPPKPGEAEAPPKHPGVLKVEAILEKVQGLEQAVDNFEGKKTDKKYLMIEEYLTKEL
LALDSVDPEGRADVRQARRDGVRKVQTILEKLEQKAIDVPGQVQVYELQPSNLEADQPLQAIMEMGAVAADKGKKNA
GNAEDPHTETQQPEATAAATSNPSSMTDTPGNPAAP
```
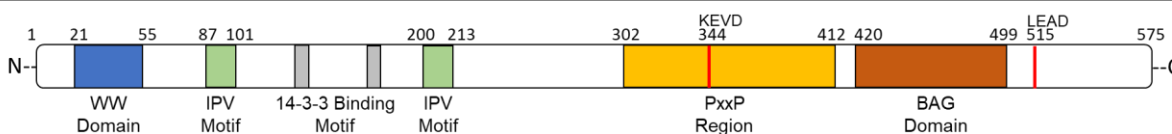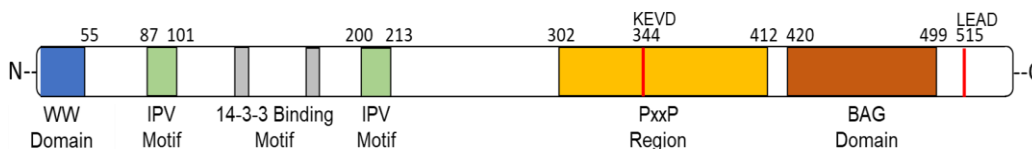BAG3-Z

D

BAG3-FL

BAG3-Z

Figure 7. Mass Spectrometry Analysis Confirms that BAG3-FL is the Endogenous Full-length BAG3 and BAG3-Z is a Truncation Product of BAG3-FL. BAG3-FL and BAG3-Z were purified by immunoprecipitation using and their amino acid sequences, in addition to that of rh-BAG3, were identified by mass spectrometry; shown in A-C are the 575 amino acids of BAG3, sequences covered by mass spectrometry are shown in green and sequences not detected are shown in red. **(A)** The amino acid structure of the purified rh-BAG3 based on combined data from mass spectrometry analysis of two samples. **(B)** The amino acid structure of BAG3-FL based on combined data from mass spectrometry analysis of four samples. **(C)** The amino acid structure of BAG3-Z based on combined data from mass spectrometry analysis of four samples. **(D)** Schematic representation of the structures of BAG3-FL and BAG3-Z based on the mass spectrometry results.

BAG3-Z Localizes to the Myofilament.

BAG3 and other members of the CASA complex localize to the Z-disk of the sarcomere in cardiomyocytes [24]. The potential reduced function of BAG3-Z would have significant negative consequences on the sarcomere PQC if BAG3-Z is able to localize to the myofilament. BAG3-Z localization to the myofilament could have further negative effects by competing with BAG3-FL. To test whether BAG3-Z is able to localize to the myofilament, human atrial and ventricular samples were homogenized and lysed in SRB/Triton-X buffer, and the cytosolic and myofilament fractions were separated by centrifugation. The myofilament protein fraction was clarified and re-suspended in 9M urea. Proteins from the cytosolic fraction were precipitated using chloroform methanol precipitation and reconstituted in 9M urea to match the buffer of the myofilament fraction. BAG3-FL and BAG3-Z in the cytosolic and myofilament fractions were analyzed by western blotting (Figure 8A). The BAG3-Z/BAG3-FL ratio was significantly higher in the myofilament-enriched fraction compared to the cytoplasmic fraction (Figure 8B). The significant increase in BAG3-Z/BAG3-FL ratio indicates preferential localization of BAG3-Z to the myofilament, and ensures the increase in BAG3-Z signal on western blots is not because of an increase in total BAG3. Our results confirm that BAG3-Z retains the ability to localize to the myofilament, despite its N- and C- termini truncations. Our findings support the possibility that

BAG3-Z could interfere with BAG3-FL at the myofilament where its impaired functions would

be pronounced, reducing the cardiomyocyte's PQC and stress response.
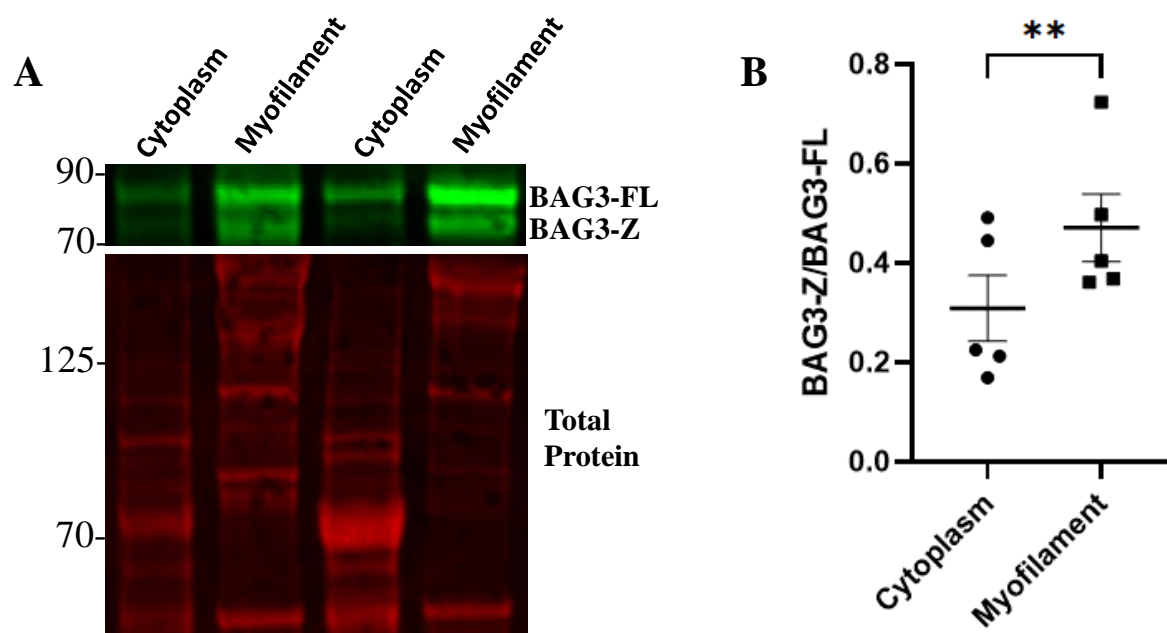
Figure 8. BAG3-Z Preferentially Localizes to the Myofilament. (A) Western blot for BAG3-FL and BAG3-Z in the cytoplasm and myofilament fractions from human atrial and ventricular tissue; image is representative of cytoplasmic and myofilament fractions from 5 human heart tissue samples **(B)** Quantification of BAG3-Z/BAG3-FL in the cytoplasmic vs myofilament fractions of human atrial and ventricular tissue samples; n = 5. Data are presented as mean ± SEM; two-tailed paired t-test.

BAG3-Z Formation is Stress Induced.

Our next goal was to uncover the mechanisms of how BAG3-FL is cleaved and BAG3-Z

is formed. Some proteins are cleaved in response to stress stimuli, such as oxidative stress, heat

shock, and DNA damage, as a result of the upregulation of certain proteases [71]. Multiple

members of the BAG family, including BAG4 and BAG6 are known to be susceptible to

cleavage [35]. BAG3 has also been shown to be cleaved by caspase 3 in response to proteasomal

stress in various cancer cell lines [33, 35, 36]. The cleavage process results in a 40 kDa C-

terminus truncation proteoform. Since BAG3 has known caspase cleavage sites and we observed

BAG3-Z in human tissue from donors with various types of cardiomyopathies and comorbidities, we hypothesized that BAG3-Z is stable stress-induced cleavage product of BAG3-FL. To test this hypothesis, we performed stress treatments on HeLa cells and neonatal rat ventricular myocytes (NRVMs). We tested proteasomal stress using the proteasome inhibitor, MG132, since it has been shown to induce the formation of the 40 kDa BAG3 proteoform. We also tested heat shock, a known activator of the Hsp70/BAG3 complex. For the proteasomal stress experiments, HeLa cells were incubated overnight in DMEM-based growth media containing 5 uM MG132 and then switched to MG132-free media and left to recover for 24 hours. For the heat shock stress, NRVMs were incubated at 42ºC for 1.5 hours then left to recover at 37ºC overnight. Cells were then harvested using trypsin, lysed in 9M urea, and BAG3 was analyzed by western blotting (Figure 9A&B). As expected, total BAG3 (summation of BAG3 proteoform bands) increased in both HeLa cells and NRVMs following stress exposure, marking the upregulation of the cellular stress response (Figure 9C&D). Excitingly, BAG3-FL was cleaved following stress exposure and BAG3-Z was observed in both cell types. The increase in BAG3-Z/BAG3-FL in the stressed cells indicates a significant increase in BAG3-FL cleavage and ensures that the increase in BAG3-Z observed by western blotting is not due to an increase in total BAG3 (Figure 9E&F). We also observed the 40 kDa BAG3 proteoform, although at a slightly higher molecular weight than previously reported, which aligns with the previous findings and confirms that our stress treatments were successful.

Although proteasomal stress and heat shock are two common treatments in cell stress experiments, they are not translational models in terms of physiological stressors that cardiomyocytes experience. To mimic physiological and pathological stress that cells experience, we tested the combination of serum starvation and hypoxia, which is used to model

ischemia/reperfusion injury [72-74]. Both HeLa and NRVMs were incubated in a low-glucose low-serum DMEM-based media and placed in a hypoxic chamber with $<1\%$ O_2 for 8-16 hours. Cells were then switched to normal growth media and left to recover in 95% O_2 incubator for 24 hours. Cells were harvested, lysed in 9M urea, and BAG3 was analyzed by western blotting (Figure 10A&E). Similar to the MG132 and heat shock stress experiments, total BAG3 was upregulated following the serum starvation/hypoxia stress treatment (Figure 10B&F). BAG3-FL was also cleaved (Figure 10C&G), and BAG3-Z formation was significantly increased following the serum starvation/hypoxia treatment, as indicated by the increase in BAG3-Z/BAG3-FL (Figure 10D&H). Together, our results show that BAG3-Z is a stable cleavage product of BAG3-FL formed under stress. It also suggests that BAG3-Z formation is associated with cellular stress and apoptosis and could worsen the cells' survival due to possible loss of function.
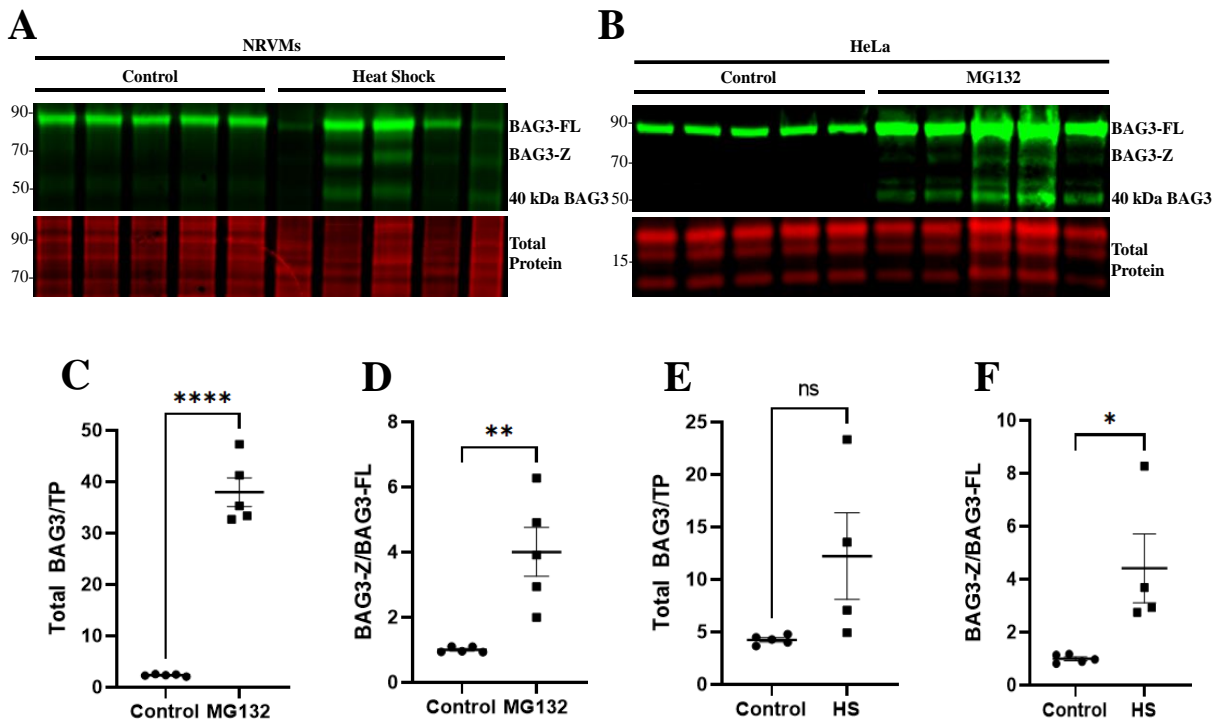
Figure 9. Proteasomal Stress and Heat Shock Trigger BAG3-FL Cleavage and BAG3-Z Formation in HeLa cells and NRVMs. (A) Western blot for control and MG132 treated HeLa cells, cells were incubated with 5µM of MG132 overnight and left to recover for 24 hours; n = 5. **(B)** Quantification of total BAG3 (summation of BAG3 proteoform bands) normalized to the total protein stain in the control vs MG132 treated cells; n = 5 **(C)** Quantification of BAG3-Z/BAG3-FL in control vs MG132 treated cells; n = 5. **(D)** Western blot for control and heat shock (HS) NRVMs, cells were incubated in a 42ºC incubator for 1.5 hours and left to recover for 24 hours; n = 5. **(E)** Quantification of total BAG3 (summation of BAG3 proteoform bands) normalized to the total protein stain in the control vs heat shock; n = 5 control and 4 heat shock. **(F)** Quantification of BAG3-Z/BAG3-FL in control vs heat shock; n = 5 control and 4 heat shock. Data are presented as mean ± SEM; two-tailed t-test.
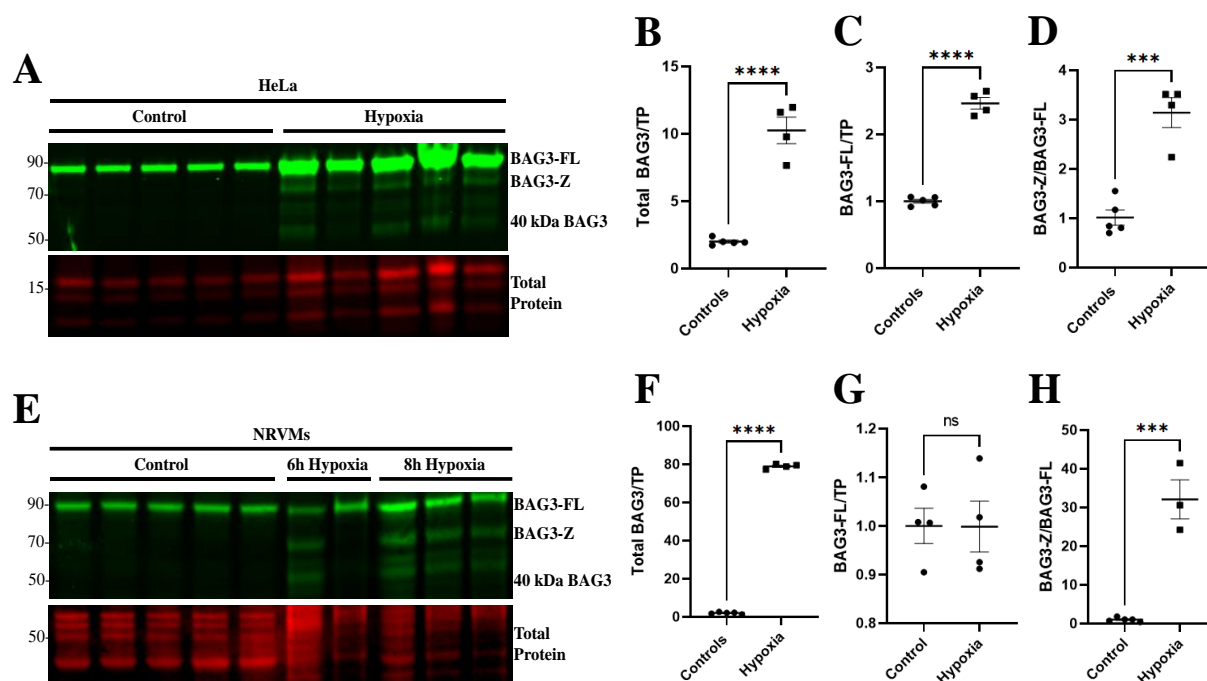
Figure 10. BAG3-Z Formation is Induced in HeLa cells and NRVMs in Response to Serum Starvation/Hypoxia Stress (HP) Treatment. (A) Western blot for control and serum starvation/hypoxia (Hypoxia) treated HeLa cells, cells were incubated with a low-glucose low-serum media in a hypoxic chamber for 18 hours and left to recover in regular media for 24 hours; n = 5. **(B)** Quantification of total BAG3 (summation of BAG3 proteoform bands) normalized to the total protein stain in the control vs treatment cells; n = 5 control and 4 treatment **(C)** Quantification of BAG3-FL normalized to the total protein stain in control vs treatment cells; n = 5 control and 4 treatment. **(D)** Quantification of BAG3-Z/BAG3-FL in control vs treatment cells; n = 5 control and 4 treatment. **(E)** Western blot for control and serum starvation/hypoxia (Hypoxia) NRVMs, cells were incubated in a low-glucose low-serum media for 6 and 8 hours then left to recover in regular media for 24 hours; n = 5. **(F)** Quantification of total BAG3 (summation of BAG3 proteoform bands) normalized to the total protein stain in the control vs treatment cells; n = 5 control and 3 treatment **(G)** Quantification of BAG3-FL normalized to the total protein stain in control vs treatment cells; n = 5 control and 3 treatment. **(H)** Quantification of BAG3-Z/BAG3-FL in control vs treatment cells; n = 5 control and 3 treatment. Data are presented as mean ± SEM; two-tailed t-test.

Identifying Proteases Responsible for BAG3-FL Cleavage and BAG3-Z Formation.

In response to cellular stressors and apoptotic stimuli, several types of proteases are upregulated and activated [71, 75]. Since we have shown that BAG3-Z formation is stress-induced, our next goal was to identify the protease/s responsible for its formation. To map out the types of proteases upregulated in response to our stress treatments, lysates of stressed HeLa cells and NRVMs expressing BAG3-Z were analyzed by mass spectrometry. Proteins from the

control and stress treatment cell lysates were prepared using an in-solution digestion protocol and cleaned up using C18 spin columns. Peptide concentrations were measured using Pierce™ Quantitative Peptide Assay kit and 500 ng - 1 ug of peptides/sample were used for mass spectrometry analysis. Analysis of the HeLa cells MG132 treatment showed the upregulation of a variety of proteases to different extents, including calpains 7 and 15, caspases 1, 2, 3, 7, 8 and cathepsins B and Z (Figure 11A). Next, we performed the same mass spectrometry analysis on control and serum starvation/hypoxia treatment HeLa and NRVMs. Results showed the upregulation of calpains 1 and 2, caspases 1, 7, 8, 9, and cathepsins B and Z in the serum starvation/hypoxia treated HeLa cells (Figure 11B). In the serum starvation/hypoxia treated NRVMs, only caspase 9 was upregulated, along with calpains 1 and 2 and cathepsins B and Z (Figure 11C). Since BAG3-Z formation was observed in HeLa cells after the MG132 and serum starvation/hypoxia stress treatments, it is likely that the same protease/s are responsible for the cleavage and would be upregulated in both stress treatments. However, it is still possible that different pathways are upregulated and activate multiple proteases that are able to cleave BAG3-FL and form BAG3-Z. By comparing the mass spectrometry results from those two treatments, we found that caspases 1, 7, and 8 were upregulated in HeLa cells after both stress treatments (Figure 13A). Adding the mass spectrometry results from the serum starvation/hypoxia NRVMs, we selected calpains 1 and 2 and caspases 1, 7, 8, and 9 as possible candidates for BAG3-Z formation.

Attempting to determine which group of proteases is responsible for BAG3-Z formation, we pre-incubated cells for 2 hours in a low-glucose/low-serum media containing 250 nM calpain inhibitor I, which inhibits calpains 1 and 2, or 20 µM calpeptin, a general calpain inhibitor. We also pretreated cells with 45 µM Z-VAD(OH)-FMK, a pan-caspase inhibitor, for 2 hours. Cells

were then incubated in a hypoxic chamber for 16 hours, switched back to normal growth media,

and left to recover overnight. We harvested the cells, lysed them in 9M urea, and analyzed

BAG3 by western blotting (Figure 12A&C). Our results showed that calpain inhibition, by both

calpain inhibitor I and calpeptin, prevented BAG3-Z formation; shown by the decrease in BAG3-

Z/BAG3-FL and increase in BAG3-FL levels in NRVMs (Figure 12B). Calpain inhibition also

prevented the increase in total BAG3 levels following the stress treatment (Figure 12B).

Pretreating the NRVMs with the pan-caspase inhibitor had similar effects on BAG3-FL cleavage

and BAG3-Z formation. Caspase inhibition significantly decreased the BAG3-Z/BAG3-FL,

indicating a reduction in BAG3-FL cleavage and BAG3-Z formation (Figure 12D). It also

rescued BAG3-FL levels and prevented the upregulation of total BAG3 (Figure 12D). Caspase

inhibition decreased BAG3-FL cleavage and BAG3-Z formation in the serum starvation/hypoxia

HeLa cells as well (Figure 12E&F).
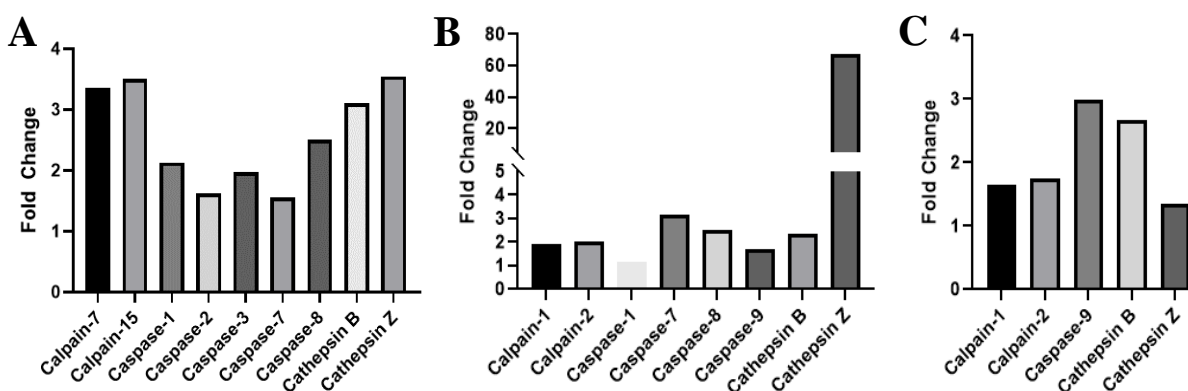
Figure 11. Various Calpains, Caspases, and Cathepsins are Upregulated in the Stressed Hela Cells and NRVMs. Graphs show the fold increase of various proteases in the stress treatment cells compared to the control cells based on mass spectrometry analysis. **(A)** Proteases upregulated in MG132 treatment HeLa cells compared to control HeLa cells; n= 5 **(B)** Proteases upregulated in the serum starvation/hypoxia (HP) treatment HeLa cells compared to control HeLa cells; n= 5 control and 3 HP **(C)** Proteases upregulated in serum starvation/hypoxia treatment NRVMs compared to control NRVMs; n =5.
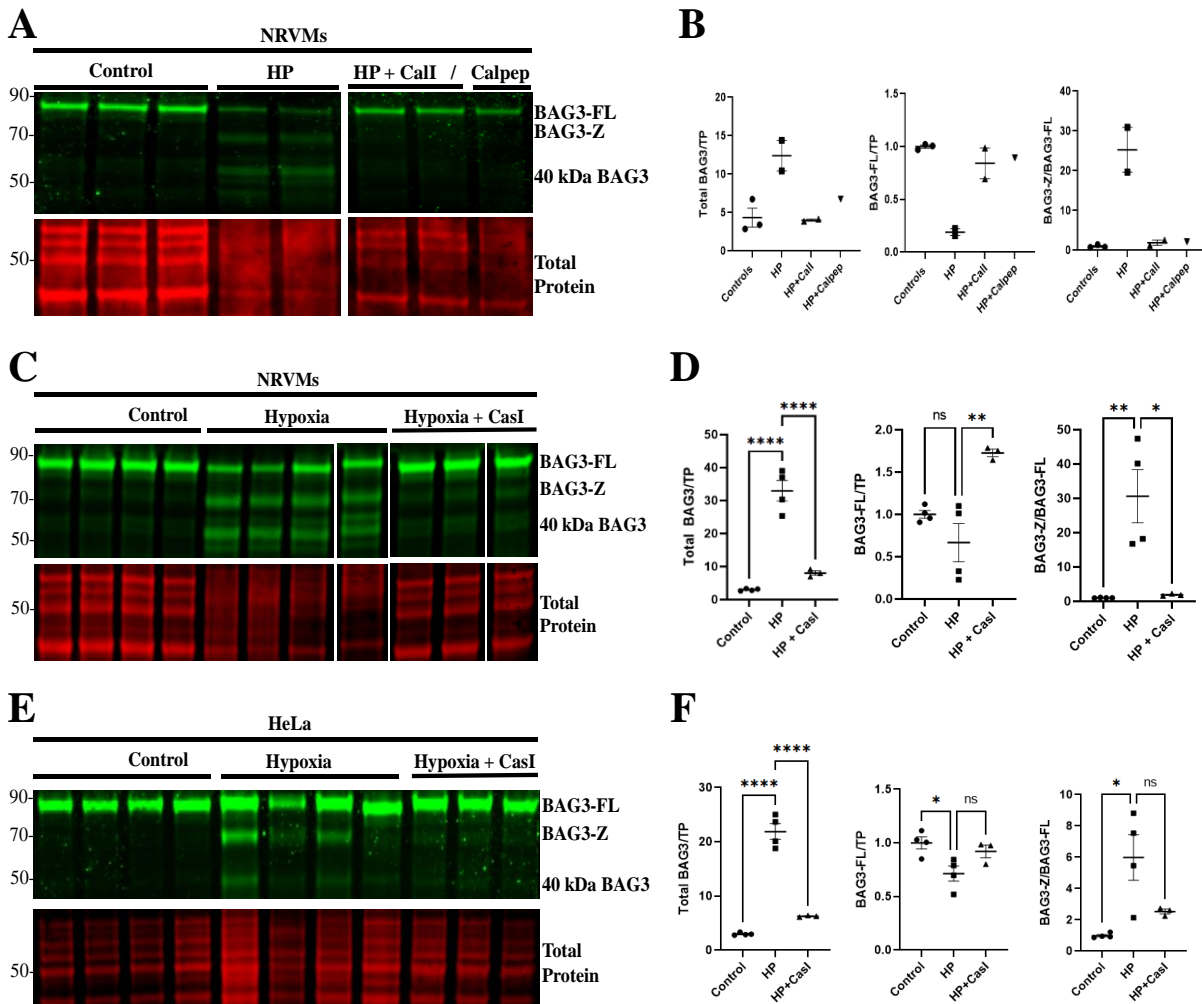
Figure 12. Calpain and Caspase Inhibition Reduces BAG3-FL Cleavage and BAG3-Z Formation in NRVMs. (A) Western blot for control, serum starvation/hypoxia (HP), and serum starvation/hypoxia with a calpain inhibitor I (HP+CalI) or calpeptin (HP+Calpep) NRVMs, cells were pre-incubated with 250 nM calpain inhibitor I or 20 µM calpeptin for 2 hours, transferred to a hypoxic chamber for 18 hours, and left to recover for 24 hours. **(B)** Quantification of total BAG3, BAG3-FL, and BAG3-Z/BAG3-FL in the control, HP, HP+CalI, and HP+Calpep; n = 3 controls, 2 HP, 2 HP+CalI and 1 HP+Calpep. **(C)** Western blot for control, serum starvation/hypoxia (HP), and serum starvation/hypoxia with a pan-caspase inhibitor (HP+CasI) NRVMs, cells were pre-incubated with 45 µM Z-VAD(OH)-FMK for 2 hours, transferred to a hypoxic chamber for 18 hours, and left to recover for 24 hours. **(D)** Quantification of total BAG3, BAG3-FL, and BAG3-Z/BAG3-FL in the control, HP, and HP+CasI; n = 4 controls, 4 HP, and 3 HP+CasI. **(E)** Western blot for control, serum starvation/hypoxia (HP), and serum starvation/hypoxia with a pan-caspase inhibitor (HP+CasI) HeLa cells, cells were pre-incubated with 45 µM Z-VAD(OH)-FMK for 2 hours, transferred to a hypoxic chamber for 18 hours, and left to recover for 24 hours. **(F)** Quantification of total BAG3, BAG3-FL, and BAG3-Z/BAG3-FL in the control, HP, and HP+CasI; n = 4 controls, 4 HP, and 3 HP+CasI. Data are presented as mean ± SEM; one-way ANOVA.

Caspases 1 and 8 Cleave BAG3-FL and Form BAG3-Z.

Taking the results from the mass spectrometry analysis and caspase inhibition

experiments, we aimed to identify the specific caspase responsible for BAG-FL cleavage and

BAG3-Z formation. BAG3 has been previously shown to be a cleavage substrate by caspase 3,

so BAG3-Z formation seemed more likely to be caspase-dependent. We performed in-vitro

cleavage assays to confirm if caspases 1, 7, and 8 can cleave BAG3-FL and form BAG3-Z. We

used caspase 3 as a positive control, since it has been shown to cleave BAG3-FL. Recombinant

human BAG3 protein (rh-BAG3) was incubated with recombinant active forms of caspases 1, 3,

7, and 8 at 37ºC for 3 hours. The reactions were stopped by adding equal amount of SDS and

reducing buffer mix and then incubating at 99ºC for 10 minutes. The products of the cleavage

reactions were analyzed by western blotting using total protein stain (Figure 13B). Caspase 1 and

8 successfully cleaved BAG3-FL at locations that generated a proteoform of similar molecular

weight to BAG3-Z. Caspase 3 cleaved BAG3-FL but only formed the 40 kDa proteoform, which

validates our cleavage assays. Caspase 7 did not cleave BAG3-FL.

We performed an in-silico analysis using Expasy PeptideCutter

(https://web.expasy.org/peptide_cutter/) looking for potential caspase cleavage sites in BAG3-

FL. The analysis did not identify any caspase cleavage sites in BAG3-FL that would result in a

proteoforms with similar molecular weight as BAG3-Z. Expasy Peptide Cutter uses canonical

caspase cleavage sites that have been previously identified. However, caspases could have

multiple other cleavage sites, especially amino acid sequences similar to the identified consensus

sequence [76]. By inspecting BAG3-FL's amino acid sequence, we identified three non-

canonical cleavage sites for caspases 1 and 8. Sites ^{38}FFVD$_{41}$ and ^{466}DSVD$_{469}$ are homologous to

the caspase 8 cleavage site, and site ^{515}LEAD$_{518}$ is homologous to the cleavage site for caspases

1 and 8. In sum, the results of the mass spectrometry analysis, the caspase inhibition experiments, and the in-vitro cleavage assays indicate that BAG3-Z formation is caspase-dependent.

A
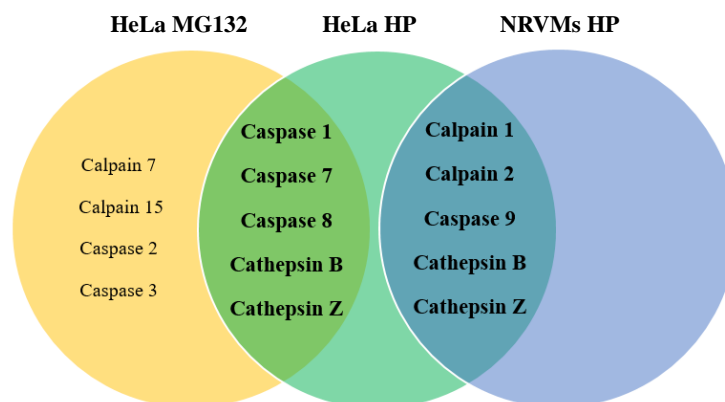
B
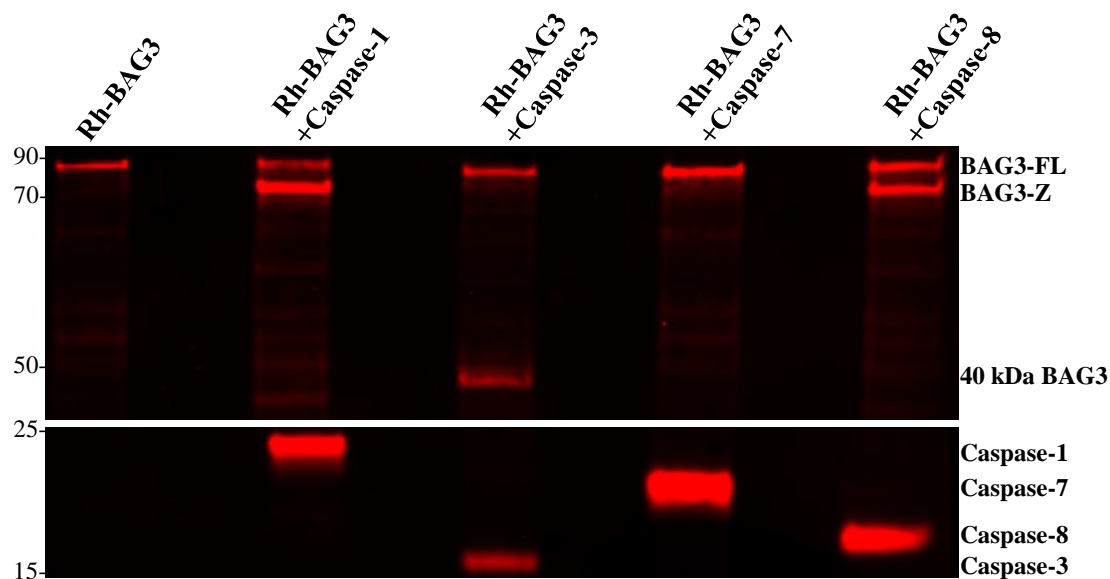
Figure 13. BAG3-FL is Cleaved by Caspases 1 and 8 to Form BAG3-Z. (A) Venn diagram showing proteases upregulated in HeLa cells following MG132 treatment and HeLa and NRVMs following serum starvation/hypoxia treatments (HP) based on mass spectrometry analysis. **(B)** Western blot with total protein stain, of the products from in-vitro cleavage assay using rh-BAG3 and recombinant active caspases, rh-BAG3 was incubated with caspases 1, 3, 7, and 8 at 37°C for 3 hours then the reaction was stopped and analyzed by western blotting.

BAG3-Z in the Failing and Non-failing Human Heart.

We initially observed BAG3-Z while comparing BAG3 in non-failing human heart samples with atrial fibrillation (Afib) and normal sinus rhythm (NSR) (Figure 14A). There was no significant difference between BAG3-Z/BAG3-FL in the Afib samples compared to the NSR (Figure 13B). Since we have established that BAG3-Z formation is stress-induced, we compared BAG3-Z in non-failing (NF) and failing heart samples with DCM. Non-failing and failing DCM human left ventricular heart samples were prepared and BAG3 in the myofilament fraction was analyzed by western blotting. We observed BAG3-Z in all the samples analyzed (Figure 14C). As has been previously reported, total BAG3 was decreased in the DCM compared to the non-failing samples (Figure 14D)[24]. However, there was no significant difference in BAG3-Z/BAG3-FL between the two groups (Figure 14G). This is likely because both BAG3-FL and BAG3-Z decreased, although not significant, in the DCM compared to the non-failing tissue (Figure 14 E&F). Our results show that BAG3-Z is also formed in non-failing and failing human heart, although its formation doesn't seem to be preferentially increased in failing hearts.
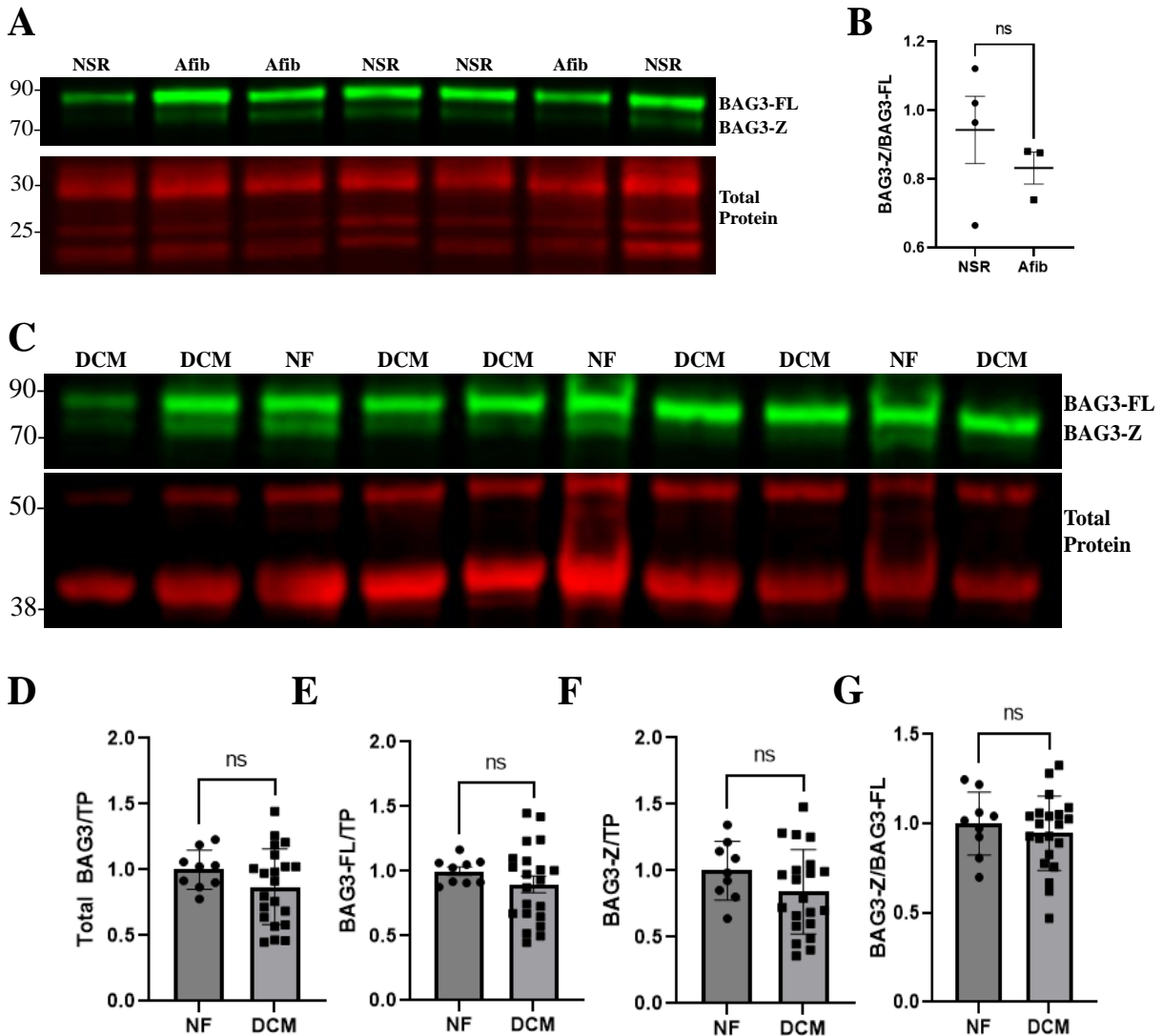
Figure 14. Total BAG3 is Reduced in DCM Compared to Non-Failing (NF) Human Ventricular Tissue, with no Difference in BAG3-Z Formation. (A) Western blot for BAG3 in the myofilament of human atrial heart samples NSR and Afib**. (B)** Quantification of BAG3-Z/BAG3-FL in the myofilament of NSR and Afib human atrial samples; n = 4 NSR and 3 Afib. **(C)** Western blot for BAG3-FL and BAG3-Z in the myofilament fraction of non-failing (NF) and DCM human left ventricular tissue; image is representative of 9 NF and 21 DCM independent samples. **(D-G)** Quantification of total BAG3 (summation of BAG3 proteoform bands), BAG3-FL, BAG3-Z, and BAG3-Z/BAG3-FL normalized to the total protein stain in the NF vs DCM samples; n = 9 NF and 21 DCM. Data are presented as mean ± SEM; two-tailed t-test.

CHAPTER FOUR

DISCUSSION

BAG3 is a multifaceted protein that is involved in a diverse number of cellular processes in different cell types [28, 58]. With growing interest in BAG3 as a target for HF therapies, it is critical to understand its structure and identify any of its proteoforms and variants. Here, we report the characterization of the full-length BAG3 protein (BAG3-FL) and the identification of a 74 kDa stress-induced cleavage product, referred to here as BAG3-Z, which has not been previously described. We found that BAG3's observed molecular weight is around 85 kDa, rather than the previously reported molecular weight of 74 kDa. The results of this study confirm that BAG3-FL, and not BAG3-Z, is the endogenous full-length form of BAG3, contrary to previous assumptions in the literature. Our results showed that BAG3-FL is not a result of BAG3-Z phosphorylation as has been hypothesized [28, 66, 67]. Treatment of human heart samples with an alkaline phosphatase did not resolve the BAG3 doublet observed. There has been a range of molecular weights reported for BAG3, from 74 kDa to 85 kDa. However, by comparing the molecular weight of BAG3 from various sources, including purified human BAG3 and BAG3 from different animal tissues and HeLa cells, we found that BAG3 consistently appears at around 85 kDa. We also surveyed references and validations reports for various BAG3 antibodies and found that that BAG3 most commonly appears at a molecular weight around 85 kDa. Altogether, our findings suggested that the proteoform observed at 85 kDa is the full-length BAG3 protein, although its calculated molecular weight is 62 kDa. Post translational modifications (PTMs) such as phosphorylation, ubiquitination, and glycosylation,

43

net charge, and protein complexes can cause proteins to have different calculated and observed molecular weights. However, the exact causes of the discrepancy between BAG3's calculated and observed molecular weights are still unknown.

Mass spectrometry analysis of rh-BAG3 and BAG3-FL and BAG3-Z extracted from human heart tissue by immunoprecipitation revealed interesting insights into the structure and regulation of BAG3. Our findings showed that both the rh-BAG3 and BAG3-FL covered more than 90% of the 575 amino acid sequence, which was an exciting discovery as it confirmed our hypothesis that BAG3-FL is indeed the endogenous full-length BAG3 protein with a molecular weight of 85 kDa. Mass spectrometry also revealed that BAG3-Z is a truncated version of BAG3-FL. BAG3-Z appears to be missing around 29 amino acids from the N-terminus and 41 amino acids from the C-terminus. Protein samples are digested by trypsin into peptides during sample preparation for mass spectrometry, so we were unable to distinguish the exact truncation site, from the trypsin cleavage site, based on the mass spectrometry results alone. However, our findings confirmed that BAG3-Z is indeed a truncated version of BAG3-FL. This is the second proteoform of BAG3 to be reported, in addition to the 40 kDa caspase cleavage product induced by proteasomal stress [33, 35, 36].

The 40 kDa BAG3 proteoform previously reported is a C-terminus cleavage where the BAG domain is lost, causing it to lose its protective role during cellular stress [36]. The partial loss of the WW domain in BAG3-Z could potentially affect its ability to interact with its protein binding partners involved in the autophagy pathway, such as p62, SYNPO2, and LC3, and impair its functions in CASA and PQC. This effect would be particularly pronounced at the myofilament, where we have shown that BAG3 preferentially localizes. Our analysis of the localization of BAG3-FL and BAG3-Z, from human atrial and ventricular tissue samples,

showed that BAG3-Z is preferentially present at the myofilament. This indicates that the N- and C-terminus truncations do not inhibit its myofilament localization, possible increasing it, and that BAG3's myofilament localization signal is likely outside of the truncated regions. The increased localization of BAG3-Z to the myofilament also indicates an attempt by the cell to upregulate the stress response and protect the sarcomere by upregulating and trafficking more BAG3 to the myofilament. However, this attempt was counteracted by BAG3-FL cleavage and BAG3-Z formation. Since BAG3-Z is a stable protein product that retained its myofilament localization, it could also compete with and act as a negative regulator of BAG3-FL. These findings suggest that BAG3-Z may interfere with the PQC functions of BAG3-FL at the myofilament, crippling the cardiomyocyte's stress response. Further studies are needed to uncover the interactome of BAG3-Z and elucidate the consequences of its truncation on autophagy, protein turnover, and the cardiomyocytes overall survival under stress.

The functions and physiological relevance of BAG3-202, the only known BAG3 splice variant, is unknown so we investigated the hypothesis that BAG3-Z is another BAG3 splice variant. We tested this hypothesis by utilizing multiple PCR experiments using BAG3 mRNA extracted from humans and a variety of BAG3 primers. We used primers that cover the full-length of each of the four exons of BAG3-FL. The PCR reactions using primers for exons 2 and 3 confirmed that the two exons are conserved in both BAG3-FL and BAG3-Z. In all human atrial and ventricular samples tested, the PCR products using primers for exons 1 and 4 yielded one product, showing that exons 1 and 4 are also conserved and that BAG3-FL and BAG3-Z are translated from the same mRNA transcript. Since the primers for exons 1 and 4 extended into the 5'UTR and 3'UTR regions, respectively, and covered the full length of the exons, our findings confirmed that BAG3-Z is not a product of alternative splicing of the BAG3-FL transcript.

An alternative candidate mechanism for BAG3-Z formation is post-translational cleavage. Stress-induced protein cleavage can generate truncated protein fragments with altered functions that play important roles in stress adaptation and survival [71]. Stress-induced protein cleavage has also been implicated in various diseases, including cancer, diabetes, and neurodegenerative diseases. BAG3 has been previously shown to be a target of caspase-dependent cleavage in multiple cancer cells [33, 35, 36]. A 40 kDa BAG3 product of caspase-dependent cleavage was observed during apoptosis caused by proteasomal stress using MG132. We tested the hypothesis that BAG3-Z is also a stable stress-induced cleavage product, by performing various stress treatments on HeLa cells and NRVMs. Total BAG3 (BAG-FL, BAG3-Z, and 40kDa BAG3) was significantly increased upon stress exposure, indicating the upregulation of the cellular stress response, as it has been previously reported [24, 65]. Interestingly, BAG3-FL was cleaved, its levels decreased, and BAG3-Z was observed in the stressed HeLa cells and NRVMs. We also observed the 40 kDa BAG3 proteoform in some of our stress experiments, aligning with previous findings and confirming that our stress treatments were successful. The decrease in the level of BAG3-FL in the stressed cells supports our hypothesis that BAG3-Z formation could be disadvantageous to the cell's stress response and PQC. If BAG3-Z's functions are impaired, its formation would sabotage the cell's attempt to respond to stress by increasing the levels of BAG3-FL. BAG3-Z hasn't been reported in the previous literature that identified the 40 kDa caspase-dependent BAG3 cleavage product. This could be attributed to the cell line, type of stress, and specificity of the BAG3 antibody used in those experiments. The 40 kDa proteoform was identified in different cancer cell lines following proteasomal stress. This proteoform is a product of BAG3 cleavage almost in half, making it easily detectable by most BAG3 antibodies. BAG3-Z is cleaved at both the N- and C- termini

and is expressed to a lesser extent compared to the 40 kDa proteoform, making it harder to detect and require antibodies with epitopes outside of the cleaved regions. Overall, our findings demonstrate that BAG3-Z is a product of stress-induced cleavage of BAG3-FL with more possibilities of negative effects on the cardiomyocytes PQC.

We utilized mass spectrometry analysis of whole cell lysates to gain an idea of the proteases upregulated in repose to our stress treatments. General analysis of the proteases upregulated in NRVMs with and without stress has not been reported before, so our mass spectrometry experiments provided new insights. Our initial stress treatments using MG132 on HeLa cells showed consistent BAG3-Z formation and high yield of proteins, so we analyzed it and used it as a reference. We then focused on the serum starvation/hypoxia stress experiments since it is the most relevant stress physiologically, especially for cardiomyocytes. Mass spectrometry analysis showed the upregulation of many calpains, caspases, and cathepsins. We compared the mass spectrometry results from the starvation/hypoxia treated NRVMs with the MG132 and starvation/hypoxia HeLa cells. By doing so, we were able to select overlapping candidates for BAG3-Z cleavage. Calpains 1 and 2, caspases 1, 7, 8, and 9 were selected as possible candidates.

It was surprising that both calpain and caspase inhibition reduced the formation of BAG3-Z. One explanation would be that inhibiting calpains inhibits apoptotic signaling that activates caspases down the line. There have been observations where inhibiting calpains lead to the inhibition of caspase activity [77-79]. For example, Powers et al. showed that calpain inhibition prevented the activation of caspases 3, 9, and 12 during cell stress [79]. This is also supported by our in-vitro cleavage assays that showed caspases 1 and 8 can cleave BAG3-FL and form BAG-Z. However, it is possible that multiple pathways cause BAG3-FL cleavage and

BAG3-Z formation. Calpains have been shown to have proteolytic activity in the myofilament, cleaving and releasing sarcomeric proteins [56]. If BAG3-FL is cleaved to form BAG3-Z by calpains upregulated during stress, it could, in turn, have negative effects on CASA and protein turnover. This means that protein turnover via calpain upregulation will have more damaging than beneficial effects on PQC and the overall cell stress response. It also means that upregulation of CASA could be less damaging to the cell than upregulating calpains in response to stress. Assessment of caspase activity after calpain inhibition as well as in-vitro cleavage assays using recombinant calpains 1 and 2 are needed to confirm this hypothesis.

We have confirmed that caspases 1 and 8 cleave BAG3-FL and form BAG3-Z, but neither caspase were upregulated in NRVMs following the serum starvation/hypoxia treatments. However, the canonical peptide cleavage sequence of caspase 9 (W/LEHD) is very homologous to that of caspases 1 (WEHD) and 8 (LETD). In-vitro cleavage assay using caspase 9 is needed to confirm its ability to form BAG3-Z. During the identification of the caspases responsible for the formation of the 40 kDa proteoform, caspases 1 and 8 were tested and BAG3-Z was not observed [36]. The recombinant BAG3 used in those in-vitro cleavage assays had a C-terminus flag tag and the cleavage products were identified on western blots using an anti-flag antibody. Since BAG3-Z is cleaved at both the N- and C- termini, the flag tag would be lost and that would explain why BAG3-Z was not identified in those experiments, further supporting our findings that the BAG3-FL cleavage that forms BAG3-Z occurs at both ends.

Although cathepsins B and Z were upregulated following our stress treatments, it is unlikely that BAG3-Z formation is cathepsin-dependent. Cathepsin B, like majority of cathepsins, localizes to endosomes and lysosomes and its upregulation is expected since the lysosomal degradation pathway is upregulated in stress [80, 81]. Cathepsin Z (also known as

cathepsin X) is also not a likely candidate since it is mainly observed in cancer cells and is a very specific carboxypeptidase, cleaving proteins only at the C-terminus [80, 82, 83]. Overall, we have confirmed that BAG3-Z formation is caspase-dependent, specifically caspases 1 and 8. More work is needed to confirm whether calpains are also capable of cleaving BAG3-FL and forming BAG3-Z.

We observed BAG3-Z in all the failing and non-failing human heart tissue samples we analyzed, which was exciting as it increased our sample number and further supported the physiological and translational relevance of BAG3-Z. It initially seemed counterintuitive to observe BAG3-Z in non-failing hearts. We have shown that BAG3-Z formation is stress-induced and possible associated with cellular stress and apoptosis, so it would be expected to find BAG3-Z mostly in the failing hearts. However, the physiological and pathological stress that the human heart experiences is more complicated than our in-vivo stress treatments on NRVMs. There are many factors, other than HF, that would be "stressful" to the heart and might explain BAG3-Z formation even in non-failing conditions. These factors include age, alcohol and tobacco consumption, mental illnesses, and other non-failing cardiovascular diseases. In our pool of 12 non-failing tissue donors, 9 were at an age between 50 and 70, and 7 were diagnosed with a cardiovascular disease, including coronary artery disease, hypertension, and atrial fibrillation. Some also suffered from other comorbidities such as drug use, stroke, and mental/psychological disorders. In collective, all these events could have stress effects on the heart and would explain the formation of BAG3-Z in the non-failing samples.

We have shown that BAG3-Z formation is associated with stress and is caspase dependent. Our findings are further supported translationally by preliminary mass spectrometry analysis of human heart tissue in which we detected caspase 1. The partial loss of the WW

domain in BAG3-Z could have negative effects on its functions, specifically its role in the autophagosome formation and protein delivery. Experiments to assess the autophagosome formation, autophagy flux, accumulation of ubiquitinated proteins, and cell survival are needed to fully understand the functions of BAG3-Z and its effects on the cell stress response. This is important clinically since we have observed BAG3-Z in a total of 33 independent human tissue samples. Verifying the exact cleavage site that forms BAG3-Z is critical for the promising BAG3-based gene therapy for HF. BAG3-gene therapy rescued cardiac function in a mouse model of HF [24]. However, the upregulated cellular stress response in the failing heart could have reduced the effectiveness of the delivered BAG3 by cleaving it and forming BAG3-Z. Successfully mutating the cleavage sites in BAG3-FL without affecting its protein interactions and functions will provide further cardioprotective effects by protecting it from stress-induced cleavage, while maintaining its CASA interactions and PQC functions. Understanding the preferential localization of BAG3-Z to the myofilament would also provide important information about BAG3 trafficking which can be used to direct the therapeutic BAG3 to the myofilament.

In conclusion, our findings provide clearer understanding of BAG3's structure and regulation in cardiomyocytes. We have identified and characterized a stress-induced cleaved BAG3 proteoform that is observed physiologically in the human heart. However, there are some limitations to our study. Neither HeLa cells nor NRVMs provide a direct link to adult human cardiomyocytes. The cellular pathways and proteases upregulated in NRVMs could be different from those upregulated in human cardiomyocytes. Our PCR experiments, even though confirmed BAG3-Z is not a splice variant, do not eliminate the possibility of it being a result of alternative translation starting sites. Although caspases 1 and 8 cleaved BAG3 in-vitro, we are yet to

confirm whether this is true in-vivo. Similar to the pan-caspase inhibitor treatments, we could

use specific inhibitors of caspases 1 and 8 and see if that will inhibit BAG3-Z formation in

response to stress. In addition, a direct assessment of the stability of BAG3-Z over time is needed

to confirm that it is a stable proteoform.

REFERENCE LIST

1.   Walter, P. and D. Ron, *The unfolded protein response: from stress pathway to homeostatic regulation.* Science, 2011. **334**(6059): p. 1081-6.

2.   Hartl, F.U., A. Bracher, and M. Hayer-Hartl, *Molecular chaperones in protein folding and proteostasis.* Nature, 2011. **475**(7356): p. 324-32.

3.   Sturner, E. and C. Behl, *The Role of the Multifunctional BAG3 Protein in Cellular Protein Quality Control and in Disease.* Frontiers in Molecular Neuroscience, 2017. **10**.

4.   Wang, X. and J. Robbins, *Heart failure and protein quality control.* Circ Res, 2006. **99**(12): p. 1315-28.

5.   Chakraborty, D., et al., *Enhanced autophagic-lysosomal activity and increased BAG3-mediated selective macroautophagy as adaptive response of neuronal cells to chronic oxidative stress.* Redox Biol, 2019. **24**: p. 101181.

6.   Vilchez, D., I. Saez, and A. Dillin, *The role of protein clearance mechanisms in organismal ageing and age-related diseases.* Nat Commun, 2014. **5**: p. 5659.

7.   Saibil, H., *Chaperone machines for protein folding, unfolding and disaggregation.* Nat Rev Mol Cell Biol, 2013. **14**(10): p. 630-42.

8.   GM, C., *The Cell: A Molecular Approach. 2nd edition. .* 2000, Sunderland (MA): Sinauer Associates.

9.   Goldberg, A.L., *Protein degradation and protection against misfolded or damaged proteins.* Nature, 2003. **426**(6968): p. 895-9.

10.   Day, S.M., *The ubiquitin proteasome system in human cardiomyopathies and heart failure.* Am J Physiol Heart Circ Physiol, 2013. **304**(10): p. H1283-93.

11.   Gain, C., et al., *Proteasomal inhibition triggers viral oncoprotein degradation via autophagy-lysosomal pathway.* PLoS Pathog, 2020. **16**(2): p. e1008105.

12.   Maejima, Y., *The critical roles of protein quality control systems in the pathogenesis of heart failure.* Journal of Cardiology, 2020. **75**(3): p. 219-227.

13.   Yerabandi, N., et al., *The role of BAG3 in dilated cardiomyopathy and its association with Charcot-Marie-Tooth disease type 2.* Acta Myol, 2022. **41**(2): p. 59-75.

14. Wang, X.J. and J. Robbins, *Heart failure and protein quality control.* Circulation Research, 2006. **99**(12): p. 1315-1328.

15. Gilda, J.E. and A.V. Gomes, *Proteasome dysfunction in cardiomyopathies.* J Physiol, 2017. **595**(12): p. 4051-4071.

16. Herrmann, J., et al., *Primary proteasome inhibition results in cardiac dysfunction.* Eur J Heart Fail, 2013. **15**(6): p. 614-23.

17. Mearini, G., et al., *The ubiquitin-proteasome system in cardiac dysfunction.* Biochim Biophys Acta, 2008. **1782**(12): p. 749-63.

18. Weekes, J., et al., *Hyperubiquitination of proteins in dilated cardiomyopathy.* Proteomics, 2003. **3**(2): p. 208-16.

19. Tian, Z., et al., *Genetically induced moderate inhibition of the proteasome in cardiomyocytes exacerbates myocardial ischemia-reperfusion injury in mice.* Circ Res, 2012. **111**(5): p. 532-42.

20. Hacihanefioglu, A., P. Tarkun, and E. Gonullu, *Acute severe cardiac failure in a myeloma patient due to proteasome inhibitor bortezomib.* Int J Hematol, 2008. **88**(2): p. 219-222.

21. Voortman, J. and G. Giaccone, *Severe reversible cardiac failure after bortezomib treatment combined with chemotherapy in a non-small cell lung cancer patient: a case report.* BMC Cancer, 2006. **6**: p. 129.

22. Grandin, E.W., et al., *Patterns of cardiac toxicity associated with irreversible proteasome inhibition in the treatment of multiple myeloma.* J Card Fail, 2015. **21**(2): p. 138-44.

23. Enrico, O., et al., *Unexpected cardiotoxicity in haematological bortezomib treated patients.* Br J Haematol, 2007. **138**(3): p. 396-7.

24. Martin, T.G., et al., *Cardiomyocyte contractile impairment in heart failure results from reduced BAG3-mediated sarcomeric protein turnover.* Nature Communications, 2021. **12**(1).

25. Feldman, A.M., et al., *Decreased Levels of BAG3 in a Family With a Rare Variant and in Idiopathic Dilated Cardiomyopathy.* Journal of Cellular Physiology, 2014. **229**(11): p. 1697-1702.

26. Fang, X., et al., *Loss-of-function mutations in co-chaperone BAG3 destabilize small HSPs and cause cardiomyopathy.* J Clin Invest, 2017. **127**(8): p. 3189-3200.

27. Doong, H., A. Vrailas, and E.C. Kohn, *What's in the 'BAG'?--A functional domain analysis of the BAG-family proteins.* Cancer Lett, 2002. **188**(1-2): p. 25-32.

28.   Rosati, A., et al., *BAG3: a multifaceted protein that regulates major cell pathways.* Cell Death & Disease, 2011. **2**.

29.   Hiebel, C., et al., *BAG3 Proteomic Signature under Proteostasis Stress.* Cells, 2020. **9**(11).

30.   Behl, C., *Breaking BAG: The Co-Chaperone BAG3 in Health and Disease.* Trends Pharmacol Sci, 2016. **37**(8): p. 672-688.

31.   Lin, H., et al., *The role of BAG3 in health and disease: A "Magic BAG of Tricks".* J Cell Biochem, 2022. **123**(1): p. 4-21.

32.   Klimek, C., et al., *BAG3-mediated proteostasis at a glance.* J Cell Sci, 2017. **130**(17): p. 2781-2788.

33.   Du, Z.X., et al., *Caspase-dependent cleavage of BAG3 in proteasome inhibitors-induced apoptosis in thyroid cancer cells.* Biochem Biophys Res Commun, 2008. **369**(3): p. 894-8.

34.   Ni, E., et al., *The PXXP domain is critical for the protective effect of BAG3 in cardiomyocytes.* Clin Exp Pharmacol Physiol, 2019. **46**(5): p. 435-443.

35.   Virador, V.M., et al., *The anti-apoptotic activity of BAG3 is restricted by caspases and the proteasome.* PLoS One, 2009. **4**(4): p. e5136.

36.   Wang, H.Q., et al., *Characterization of BAG3 cleavage during apoptosis of pancreatic cancer cells.* J Cell Physiol, 2010. **224**(1): p. 94-100.

37.   Kathage, B., et al., *The cochaperone BAG3 coordinates protein synthesis and autophagy under mechanical strain through spatial regulation of mTORC1.* Biochim Biophys Acta Mol Cell Res, 2017. **1864**(1): p. 62-75.

38.   Merabova, N., et al., *WW Domain of BAG3 Is Required for the Induction of Autophagy in Glioma Cells.* Journal of Cellular Physiology, 2015. **230**(4): p. 831-841.

39.   Kirk, J.A., J.Y. Cheung, and A.M. Feldman, *Therapeutic targeting of BAG3: considering its complexity in cancer and heart disease.* J Clin Invest, 2021. **131**(16).

40.   Klimek, C., et al., *The Hippo network kinase STK38 contributes to protein homeostasis by inhibiting BAG3-mediated autophagy.* Biochim Biophys Acta Mol Cell Res, 2019. **1866**(10): p. 1556-1566.

41.   Ji, C., et al., *BAG3 and SYNPO (synaptopodin) facilitate phospho-MAPT/Tau degradation via autophagy in neuronal processes.* Autophagy, 2019. **15**(7): p. 1199-1213.

42.   Cristofani, R., et al., *The Role of HSPB8, a Component of the Chaperone-Assisted Selective Autophagy Machinery, in Cancer.* Cells, 2021. **10**(2).

43.   Dimauro, I., et al., *The role of alphaB-crystallin in skeletal and cardiac muscle tissues.* Cell Stress Chaperones, 2018. **23**(4): p. 491-505.

44.   Hishiya, A., et al., *BAG3 directly interacts with mutated alphaB-crystallin to suppress its aggregation and toxicity.* PLoS One, 2011. **6**(3): p. e16828.

45.   Rauch, J.N., et al., *BAG3 Is a Modular, Scaffolding Protein that physically Links Heat Shock Protein 70 (Hsp70) to the Small Heat Shock Proteins.* J Mol Biol, 2017. **429**(1): p. 128-141.

46.   Ganassi, M., et al., *A Surveillance Function of the HSPB8-BAG3-HSP70 Chaperone Complex Ensures Stress Granule Integrity and Dynamism.* Mol Cell, 2016. **63**(5): p. 796-810.

47.   Xu, Z., et al., *14-3-3 protein targets misfolded chaperone-associated proteins to aggresomes.* J Cell Sci, 2013. **126**(Pt 18): p. 4173-86.

48.   Doong, H., et al., *CAIR-1/BAG-3 forms an EGF-regulated ternary complex with phospholipase C-gamma and Hsp70/Hsc70.* Oncogene, 2000. **19**(38): p. 4385-95.

49.   Qu, H.Q., A.M. Feldman, and H. Hakonarson, *Genetics of BAG3: A Paradigm for Developing Precision Therapies for Dilated Cardiomyopathies.* Journal of the American Heart Association, 2022. **11**(23).

50.   Minoia, M., et al., *BAG3 induces the sequestration of proteasomal clients into cytoplasmic puncta Implications for a proteasome-to-autophagy switch.* Autophagy, 2014. **10**(9): p. 1603-1621.

51.   Jaffer, F., et al., *BAG3 mutations: another cause of giant axonal neuropathy.* Journal of the Peripheral Nervous System, 2012. **17**(2): p. 210-216.

52.   Gamerdinger, M., et al., *BAG3 mediates chaperone-based aggresome-targeting and selective autophagy of misfolded proteins.* Embo Reports, 2011. **12**(2): p. 149-156.

53.   Baldan, S., et al., *The Hsp70-Bag3 complex modulates the phosphorylation and nuclear translocation of Hippo pathway protein Yap.* J Cell Sci, 2021. **134**(23).

54.   Martin, T.G., et al., *BAG3 expression and sarcomere localization in the human heart are linked to HSF-1 and are differentially affected by sex and disease.* American Journal of Physiology-Heart and Circulatory Physiology, 2021. **320**(6): p. H2339-H2350.

55.   Arndt, V., et al., *Chaperone-assisted selective autophagy is essential for muscle maintenance.* Curr Biol, 2010. **20**(2): p. 143-8.

56. Martin, T.G. and J.A. Kirk, *Under construction: The dynamic assembly, maintenance, and degradation of the cardiac sarcomere.* Journal of Molecular and Cellular Cardiology, 2020. **148**: p. 89-102.

57. Selcen, D., et al., *Mutation in BAG3 causes severe dominant childhood muscular dystrophy.* Ann Neurol, 2009. **65**(1): p. 83-9.

58. Myers, V.D., et al., *The Multifunctional Protein BAG3 A Novel Therapeutic Target in Cardiovascular Disease.* Jacc-Basic to Translational Science, 2018. **3**(1): p. 122-131.

59. Zhou, J., et al., *Cyclin-Dependent Kinase 5-Dependent BAG3 Degradation Modulates Synaptic Protein Turnover.* Biol Psychiatry, 2020. **87**(8): p. 756-769.

60. *Uniprot C9JFK9.* Available from: https://www.uniprot.org/uniprotkb/C9JFK9/entry.

61. Dominguez, F., et al., *Dilated Cardiomyopathy Due to BLC2-Associated Athanogene 3 (BAG3) Mutations.* Journal of the American College of Cardiology, 2018. **72**(20): p. 2471-2481.

62. Fang, X., et al., *Loss-of-function mutations in co-chaperone BAG3 destabilize small HSPs and cause cardiomyopathy.* Journal of Clinical Investigation, 2017. **127**(8): p. 3189-3200.

63. Kimura, K., et al., *Overexpression of human BAG3(P209L) in mice causes restrictive cardiomyopathy.* Nat Commun, 2021. **12**(1): p. 3575.

64. Bruno, A.P., et al., *Identification of a synaptosome-associated form of BAG3 protein.* Cell Cycle, 2008. **7**(19): p. 3104-5.

65. Pagliuca, M.G., et al., *Regulation by heavy metals and temperature of the human BAG-3 gene, a modulator of Hsp70 activity.* Febs Letters, 2003. **541**(1-3): p. 11-15.

66. Rosati, A., et al., *Role of BAG3 protein in leukemia cell survival and response to therapy.* Biochimica Et Biophysica Acta-Reviews on Cancer, 2012. **1826**(2): p. 365-369.

67. Rosati, A., et al., *Apoptosis inhibition in cancer cells: A novel molecular pathway that involves BAG3 protein.* International Journal of Biochemistry & Cell Biology, 2007. **39**(7-8): p. 1337-1342.

68. Gentilella, A. and K. Khalili, *Autoregulation of co-chaperone BAG3 gene transcription.* J Cell Biochem, 2009. **108**(5): p. 1117-24.

69. Luthold, C., et al., *CDK1-Mediated Phosphorylation of BAG3 Promotes Mitotic Cell Shape Remodeling and the Molecular Assembly of Mitotic p62 Bodies.* Cells, 2021. **10**(10).

70. Singh, P. and E.P. Ahi, *The importance of alternative splicing in adaptive evolution.* Mol Ecol, 2022. **31**(7): p. 1928-1938.

71. Fulda, S., et al., *Cellular stress responses: cell survival and cell death.* Int J Cell Biol, 2010. **2010**: p. 214074.

72. Son, E., et al., *The optimal model of reperfusion injury in vitro using H9c2 transformed cardiac myoblasts.* Korean J Physiol Pharmacol, 2020. **24**(2): p. 173-183.

73. Chen, H., et al., *Lysophosphatidic Acid Pretreatment Attenuates Myocardial Ischemia/Reperfusion Injury in the Immature Hearts of Rats.* Front Physiol, 2017. **8**: p. 153.

74. Bonavita, F., et al., *H9c2 cardiac myoblasts undergo apoptosis in a model of ischemia consisting of serum deprivation and hypoxia: inhibition by PMA.* FEBS Lett, 2003. **536**(1-3): p. 85-91.

75. Harwood, S.M., M.M. Yaqoob, and D.A. Allen, *Caspase and calpain function in cell death: bridging the gap between apoptosis and necrosis.* Ann Clin Biochem, 2005. **42**(Pt 6): p. 415-31.

76. Green, D.R., *Caspases and Their Substrates.* Cold Spring Harbor Perspectives in Biology, 2022. **14**(3).

77. McCollum, A.T., P. Nasr, and S. Estus, *Calpain activates caspase-3 during UV-induced neuronal death but only calpain is necessary for death.* J Neurochem, 2002. **82**(5): p. 1208-20.

78. Nakajima, E., et al., *Activation of the mitochondrial caspase pathway and subsequent calpain activation in monkey RPE cells cultured under zinc depletion.* Eye (Lond), 2014. **28**(1): p. 85-92.

79. Nelson, W.B., et al., *Cross-talk between the calpain and caspase-3 proteolytic systems in the diaphragm during prolonged mechanical ventilation.* Crit Care Med, 2012. **40**(6): p. 1857-63.

80. Cavallo-Medved, D., K. Moin, and B. Sloane, *Cathepsin B: Basis Sequence: Mouse.* AFCS Nat Mol Pages, 2011. **2011**.

81. Cheng, X.W., et al., *Role for cysteine protease cathepsins in heart disease: focus on biology and mechanisms with clinical implication.* Circulation, 2012. **125**(12): p. 1551-62.

82. Allan, E.R.O., et al., *A role for cathepsin Z in neuroinflammation provides mechanistic support for an epigenetic risk factor in multiple sclerosis.* J Neuroinflammation, 2017. **14**(1): p. 103.

83.   Nagler, D.K., et al., *Human cathepsin X: A cysteine protease with unique carboxypeptidase activity.* Biochemistry, 1999. **38**(39): p. 12648-54.

VITA

       The author, Ahmed, was born in Saudi Arabia on July 10, 1998 to Gamal Zied and Aziza Mohamed. He attended Iowa State University, Iowa where he earned a Bachelor's of Science, summa cum laude, in Kinesiology and Health in December 2020. After graduation, Ahmed matriculated into the Loyola University Chicago Stritch School of Medicine Masters Graduate Program, and began his graduate education in the Cell and Molecular Physiology Program under the mentorship of Dr. Jonathan Kirk.

       After completion of his graduate studies, Ahmed will be the lab manager for the Kirk Lab at Loyola University Chicago.